universe

MDPI

Article

Cubic Geometric Inflation with Radiation and a Minimally Coupled Scalar Field: Dynamical-Systems Analysis and Inflationary Diagnostics

Luciano Navarro-Coydán [1], J. Alberto Vázquez [2], Israel Quiros [3] and Ricardo García-Salcedo [4,*]

[1] Departamento de Física Teórica, Facultad de Física, Universidad de Valencia, 46100 Burjassot, Spain; manacoy@alumni.uv.es
[2] Instituto de Ciencias Físicas, Universidad Nacional Autónoma de México, Cuernavaca 62210, Mexico; javazquez@icf.unam.mx
[3] Departamento de Ingeniería Civil, División de Ingeniería, Universidad de Guanajuato, Guanajuato 36000, Mexico; i.quiros@ugto.mx
[4] Centro de Investigación en Ciencia Aplicada y Tecnología Avanzada, Unidad Legaria del Instituto Politécnico Nacional, Legaria 694, Ciudad de Mexico 11500, Mexico
* Correspondence: rigarcias@ipn.mx

Abstract

We investigate the background dynamics of cubic Geometric Inflation coupled with radiation and a minimally coupled canonical scalar field with an exponential potential, using the cubic truncation as a minimal test of geometric-to-scalar inflationary cascades. We formulate the cosmological equations as an autonomous dynamical system and analyze its finite critical points and representative Hubble-flow trajectories. The cubic sector can generate an initial geometrically accelerated phase, but its duration grows only logarithmically with the initial curvature hierarchy and is insufficient to solve the horizon problem for moderate initial conditions. The subsequent scalar-field-dominated stage obeys the power-law relation $r \simeq 8(1-n_s)$ under the standard GR-based first-order mapping, placing it in strong tension with current bounds on primordial tensor modes. Moreover, no value of the constant exponential-potential slope yields a graceful exit into a standard radiation-dominated epoch. The regular branch requires trans-Planckian radiation densities in the asymptotic past, whereas the alternative branch contains a finite-curvature dynamical degeneracy. Thus, although cascade-like background trajectories exist, the minimal cubic model does not satisfy the basic background requirements of a viable inflationary cosmology.

Keywords: cosmology; dynamical systems; geometric inflation; extended theories of gravity; Hubble slow-roll (horizon-flow) parameters

Check for updates

Academic Editors: Lorenzo Iorio and Yi-Fu Cai

Received: 22 July 2026
Revised: 2 October 2026
Accepted: 6 October 2026
Published: 15 October 2026

Copyright: © 2026 by the authors. Licensee MDPI, Basel, Switzerland. This article is an open access article distributed under the terms and conditions of the Creative Commons Attribution (CC BY) license.

1. Introduction

Inflation remains one of the most extensively studied frameworks for describing the physics of the very early Universe. In its standard form, a quasi-de Sitter stage is driven by a scalar degree of freedom, the inflaton, whose potential energy dominates the total energy density. This mechanism solves several conceptual problems of the hot Big Bang model, such as the horizon, flatness, and monopole problems, and it also provides a causal origin for the primordial scalar perturbations that seed the large-scale structure of the Universe [1–3]. The Cosmic Microwave Background (CMB) observations are consistent with a nearly scale-invariant scalar spectrum and predominantly adiabatic primordial perturbations [4]. The subsequent evolution of primordial adiabatic perturbations and

their imprint on the CMB were already established in the seminal analyses of Peebles and Yu [5] and Sunyaev and Zel'dovich [6]. While these properties arise naturally in many inflationary scenarios, CMB observations alone do not uniquely identify inflation as the mechanism that generated the initial primordial conditions [7,8]. Nevertheless, important theoretical questions remain open. Among them are the microscopic origin of the inflaton, the naturalness and shape of its potential, the sensitivity to initial conditions, the trans-Planckian problem associated with modes whose physical wavelengths may have been sub-Planckian at the beginning of inflation, and the need for a consistent mechanism of graceful exit and reheating [9–12].

These open issues motivate exploring inflationary scenarios in which the early accelerated expansion is not attributed solely to a fundamental scalar field, but may instead arise from the gravitational sector itself. This possibility is particularly natural at very high curvatures, where the Einstein–Hilbert action is expected to receive corrections. From the viewpoint of effective field theory, quantum gravity, or string-inspired models, higher-order curvature invariants generically appear in the gravitational action. Classic examples include quadratic curvature corrections, such as those appearing in Starobinsky inflation, as well as more general higher-curvature terms motivated by renormalization, effective actions, and low-energy string corrections [13–15]. Therefore, the early Universe provides a natural arena in which to test whether high-curvature geometric corrections can produce, or at least contribute to, inflationary dynamics.

A particularly interesting class of higher-curvature theories is provided by Generalized Quasi-Topological Gravities (GQTG). These are theories whose action is built from a finite or infinite tower of Lagrangian densities constructed from contractions of the Riemann tensor and the metric, without covariant derivatives,

$$S = \frac{1}{2\kappa^2}\int d^4x\sqrt{-g}\left[\alpha_1 R + \sum_{n=3}^{\infty}\alpha_n \mathcal{R}_{(n)}\right], \tag{1}$$

where R is the Ricci scalar and $\mathcal{R}_{(n)}$ denotes a curvature invariant of order n. These theories satisfy two main conditions: (i) the linearized field equations around any maximally symmetric spacetime propagate only the transverse-traceless massless graviton in vacuum, up to a redefinition of Newton's constant, and (ii) the equations of motion for a static spherically symmetric black hole are second-order [16,17]. The cosmological GQTG sector has been constructed in accordance with criteria for a viable cosmological theory [18]. This cosmological sector, commonly referred to as Geometric Cosmology (GC), has the following characteristics: (1) its action is compatible with Equation (1), (2) it modifies the Einstein field equations in a non-trivial way in $Dim = 4$, and (3) it leads to second-order cosmological equations on homogeneous and isotropic backgrounds, while also preserving well-behaved static and spherically symmetric sectors.

The modified Friedmann equations [19–22], for a perfect fluid with energy density ρ and pressure p, are

$$3F(H) = \kappa^2\rho, \quad -\frac{\dot{H}}{H}F'(H) = \kappa^2(\rho + p), \tag{2}$$

$$F'(H) \equiv \partial_H F(H), \quad F(H) = H^2 + \sum_{n=3}^{\infty}\alpha_n H^{2n}, \tag{3}$$

where the expansion history of the Universe is controlled by a function of the Hubble parameter, $F(H)$, generated by a tower of higher-curvature invariants. In the early Universe, this framework gives rise to Geometric Inflation (GI), in which curvature corrections rather than an inflaton field drive inflation. The simplest non-trivial realization of this idea is the cubic curvature sector, closely related to Cosmological Einsteinian Cubic Gravity

(CECG) [19,23]. In a spatially flat Friedmann–Lemaître–Robertson–Walker (FLRW) background, the cubic truncation modifies the Friedmann equations while preserving their second-order character.

These solutions have also been explored using dynamical-systems methods, showing that the CECG dynamics are well-posed as an initial-value problem [24]. Moreover, for the complete tower of higher-order curvature invariants, it has been shown that the GI framework may provide a quantum origin for primordial inflation [25]. At the background level, several early-Universe GI models have been analyzed through their slow-roll parameters, with some trajectories found to be compatible with the marginalized 95% confidence-level regions reported by the Planck Collaboration [26]. In addition, observational statistical analyses in the late-time cosmological regime indicate that certain Geometric Cosmology models can fit current data [27].

Although GI and Geometric Cosmology provide an attractive mechanism for describing the early accelerated stage and, in some extensions, the main epochs of cosmic evolution, Ref. [28] pointed out three important issues. First, in the cubic case, in the de Sitter scenario, small anisotropies may develop and trigger an instability [29], thereby challenging the GI mechanism. Second, in the purely geometric scenario with radiation, the high-curvature regime may require an excessively large radiation density. Indeed, if the geometric function $F(H)$ diverges as $H \to \infty$, the corresponding radiation density needed to source the early accelerated stage can become trans-Planckian. This challenges the physical interpretation of the initial regime and raises questions about the validity of the effective description. Third, a purely geometric model does not automatically provide a standard reheating mechanism. Because the geometric sector does not correspond to an oscillating matter field with explicit decay channels, it is unclear how the energy stored during inflation converts into a hot radiation bath after inflation.

A possible way to address these difficulties was proposed in Ref. [28]. The basic idea is that radiation can modify the high-curvature background evolution, while a scalar field may provide an additional dynamical component that can participate in the exit from the initial geometric stage. In such a scenario, the early acceleration may begin as a geometrically driven phase, after which the scalar field becomes dynamically relevant and can control the subsequent evolution. This motivates studying a hybrid configuration in which the cubic geometric sector, radiation, and a scalar field coexist at the background level.

Our main objective is to analytically and dynamically evaluate the cubic truncation of Geometric Inflation with radiation and a minimally coupled scalar field, understood as a minimal background-level test case, to determine whether the transition between a high-curvature geometric stage and a subsequent scalar stage can achieve a geometric-scalar cascade compatible with the basic requirements of inflationary cosmology. In particular, we focus on identifying the obstacles to sufficient geometric e-folds, compatible inflationary diagnostics, a graceful exit, and a transition to a standard radiative era, before considering the full higher-curvature tower, non-minimal couplings, or more general scalar potentials. The aim is not to claim full phenomenological viability, but to identify which obstructions already arise in the minimal setting.

To this end, we introduce a compactified Hubble variable together with dimensionless scalar-field variables that encode the relative contributions of the geometric sector, the scalar kinetic energy, and the scalar potential energy. We then determine the finite critical points of the system, analyze their stability, and examine the leading asymptotic behavior of the non-compact positive-coupling branch. We also compute the Hubble-flow parameters along representative trajectories. Our goal is therefore not only to identify the possible asymptotic regimes of the model, but also to assess whether this minimal hybrid realization has enough dynamical freedom to approach a phenomenologically acceptable inflationary background.

We perform the analysis at the level of the homogeneous and isotropic background. The comparison with CMB constraints is therefore understood as a preliminary GR-based Hubble-flow diagnostic rather than a complete perturbative prediction. In particular, we use the standard first-order GR-based relations between the Hubble-flow parameters and the scalar spectral index n_s and tensor-to-scalar ratio r to assess whether the background evolution can approach a quasi-de Sitter regime compatible with the adopted observational constraints. A full confrontation with CMB data in a higher-curvature theory would require deriving the scalar and tensor perturbation sectors, including the corresponding kinetic coefficients and propagation speeds. Accordingly, the present work should be understood as a background-level viability analysis of the proposed hybrid cubic model.

This paper is organized as follows. In Section 2, we present the cubic geometric-inflation model coupled to radiation and a minimally coupled scalar field, and derive the corresponding background equations. In Section 3, we analytically examine the cubic geometric sector in order to determine its inflationary potential, the duration of the geometrically accelerated stage, and the main obstructions already present at the background level. In Section 4, we introduce the compactified Hubble variable and the dimensionless scalar-field variables, formulate the autonomous dynamical system, analyze the leading asymptotic behavior of the non-compact positive-coupling branch, discuss the effective-fluid background diagnostics, and compute the Hubble-flow parameters. In Section 5, we analyze the critical points, their stability, and the associated effective cosmological regimes, and discuss the resulting tension with the adopted observational ranges of n_s and r. Finally, in Section 6, we summarize our results and discuss the implications for the cubic truncation and for possible extensions involving the full geometric-inflation tower.

2. Cubic Truncation of Geometric Inflation and Cosmological Equations

GI can be formulated as an effective theory of gravity built from higher-curvature densities constructed solely from contractions of the Riemann tensor and the metric. In its simplest (cubic) realization, one considers the four-dimensional CECG model, whose dynamics are generated by the cubic combination relevant for the Cosmological Einsteinian Cubic Gravity sector:

$$\mathcal{R}_{(3)} \equiv \mathcal{P} - 8\mathcal{C}, \tag{4}$$

where $\mathcal{P}$ is the Einsteinian cubic invariant and $\mathcal{C}$ is an additional cubic scalar. Their explicit forms are [30]:

$$\mathcal{P} = 12R_{\mu\ \lambda}^{\ \nu\ \sigma}R_{\nu\ \sigma}^{\ \tau\ \rho}R_{\tau\ \rho}^{\ \mu\ \lambda} + R_{\mu\lambda}^{\ \ \nu\sigma}R_{\nu\sigma}^{\ \ \tau\rho}R_{\tau\rho}^{\ \ \mu\lambda} - 12R_{\mu\lambda\nu\sigma}R^{\mu\nu}R^{\lambda\sigma} + 8R_{\mu}^{\ \lambda}R_{\lambda}^{\ \nu}R_{\nu}^{\ \mu}, \tag{5}$$

$$\mathcal{C} = R_{\mu\lambda\nu\sigma}R^{\mu\lambda\nu}_{\ \ \ \ \tau}R^{\sigma\tau} - \frac{1}{4}RR_{\mu\lambda\nu\sigma}R^{\mu\lambda\nu\sigma} - 2R_{\mu\lambda\nu\sigma}R^{\mu\nu}R^{\lambda\sigma} + \frac{1}{2}RR_{\mu\nu}R^{\mu\nu}. \tag{6}$$

In the conventions of Ref. [24], the action reads

$$S = \frac{1}{2\kappa^2}\int d^4x\,\sqrt{-g}\Big[R + 2\beta\,\mathcal{R}_{(3)} + 2\kappa^2\mathcal{L}_m\Big], \tag{7}$$

with $\beta \in \mathbb{R}$ denoting the cubic coupling. The cosmological constant is not included, since it plays no role in the early-Universe dynamics considered in this work. The sign of β selects different cosmological branches, as discussed below.

The matter Lagrangian is taken as

$$\mathcal{L}_m = \mathcal{L}_r + \mathcal{L}_\phi, \qquad \mathcal{L}_\phi = -\frac{1}{2}g^{\mu\nu}\partial_\mu\phi\,\partial_\nu\phi - V(\phi), \tag{8}$$

where $\mathcal{L}_r$ represents a radiation-perfect fluid, minimally coupled to curvature, and $\mathcal{L}_\phi$ is the Lagrangian density of a canonical scalar field ϕ with potential $V(\phi)$, yielding

$$T^{(\phi)}_{\mu\nu} = \partial_\mu\phi\,\partial_\nu\phi - g_{\mu\nu}\left[\frac{1}{2}(\partial\phi)^2 + V(\phi)\right]. \tag{9}$$

The corresponding field equations can be written in compact Euler–Lagrange form as

$$G_{\mu\nu} + 2\beta\left[\left(\frac{\partial\mathcal{R}_{(3)}}{\partial R^{\mu\alpha\beta\sigma}}\right)R_\nu{}^{\alpha\beta\sigma} - \frac{1}{2}g_{\mu\nu}\mathcal{R}_{(3)} - 2\nabla^\alpha\nabla^\beta\left(\frac{\partial\mathcal{R}_{(3)}}{\partial R^{\mu\alpha\beta\nu}}\right)\right] = \kappa^2 T_{\mu\nu}, \tag{10}$$

where $T_{\mu\nu} = T^{(r)}_{\mu\nu} + T^{(\phi)}_{\mu\nu}$.

We now specialize to a spatially flat FLRW spacetime,

$$ds^2 = -dt^2 + a^2(t)\delta_{ij}dx^i dx^j, \qquad H \equiv \frac{\dot{a}}{a}. \tag{11}$$

In this background, $F(H) = H^2 + 16\beta H^6$ and the cosmological equations remain second-order in time derivatives and take the form

$$3H^2\left(1 + 16\beta H^4\right) = \kappa^2\rho, \tag{12}$$

$$2\dot{H}\left(1 + 48\beta H^4\right) = -\kappa^2(\rho + p), \tag{13}$$

together with the standard conservation law

$$\dot{\rho} + 3H(\rho + p) = 0. \tag{14}$$

For the matter sector we take $\rho = \rho_r + \rho_\phi$ and $p = p_r + p_\phi$, with

$$\rho_\phi = \frac{1}{2}\dot{\phi}^2 + V(\phi), \qquad p_\phi = \frac{1}{2}\dot{\phi}^2 - V(\phi), \qquad p_r = \omega_r\rho_r, \qquad \omega_r = \frac{1}{3}, \tag{15}$$

and the scalar-field equation of motion

$$\ddot{\phi} + 3H\dot{\phi} + V_{,\phi} = 0. \tag{16}$$

It is convenient to rewrite Equations (12) and (13) in an "effective-fluid" form, which is a formal rearrangement of the field equations and not an independent material fluid, by moving the higher-curvature contributions to the right-hand side:

$$3H^2 = \kappa^2(\rho + \rho_{\mathrm{GI3}}), \qquad \rho_{\mathrm{GI3}} = -\frac{48\beta}{\kappa^2}H^6, \tag{17}$$

$$2\dot{H} = -\kappa^2[(\rho + p) + (\rho_{\mathrm{GI3}} + p_{\mathrm{GI3}})], \qquad p_{\mathrm{GI3}} = \frac{48\beta}{\kappa^2}H^6 + \frac{96\beta}{\kappa^2}H^4\dot{H}, \tag{18}$$

which explicitly shows that the cubic sector contributes to an effective energy density and pressure. This rewriting is useful for the dynamical interpretation of the model, although it should not be understood as introducing an additional component of physical matter.

For the dynamical-system analysis below, we work in reduced Planck units, $\kappa^2 = 1$. In these units, the logarithmic slope of the scalar potential used below is dimensionless.

In the present work, we assume an exponential potential, $V(\phi) = V_0 e^{-\gamma\phi}$, characterized by the constant dimensionless slope parameter γ. This choice keeps the system autonomous and analytically tractable. A realistic reheating mechanism would require a potential with a minimum, for which the logarithmic slope $-V_{,\phi}/V$ becomes field-dependent. Such an extension would require enlarging the phase space by introducing either ϕ or

an equivalent slope variable as an additional dynamical degree of freedom and will be addressed in future work. A multi-exponential potential represents one possible realization of such a field-dependent logarithmic slope and could relax the constant-slope power-law obstruction found below. In particular, a double-exponential potential can interpolate between different effective slopes during the scalar-field evolution. However, a standard sum of positive decreasing exponentials is generally monotonic and does not by itself provide the minimum or energy-transfer mechanism required for a conventional reheating phase. A detailed assessment of this possibility therefore requires an enlarged dynamical system and lies beyond the scope of the present work. Thus, the exponential potential should be regarded here as a minimal closure assumption that allows for a global phase-space analysis, rather than as a complete model of reheating or post-inflationary dynamics.

In what follows, we focus on the early-time inflationary regime, with the matter sector restricted to radiation and the minimally coupled scalar field introduced above. The dynamics are therefore governed by radiation, the scalar degree of freedom, and the cubic curvature correction. This setup is consistent with the main purpose of the present work, namely, to assess the background-level viability of a minimal hybrid cubic geometric-inflation scenario.

3. Analytic Structure of the Cubic Geometric Sector

Before introducing the full autonomous system, we should understand the cubic sector as a minimal dynamical benchmark rather than a complete ultraviolet description. It provides the simplest setting in which one can test whether a high-curvature geometric correction can initiate an accelerated stage and whether adding radiation and a minimally coupled scalar field can connect that stage to a viable scalar-field epoch. In this way, it is useful to isolate the analytic properties of the purely geometric cubic sector. This preliminary step is necessary for two reasons. First, it lets us determine what the cubic correction can and cannot do before including the scalar field. Second, it clarifies which features of the phase-space flow are genuine dynamical effects of the coupled system and which ones are already encoded in the modified Friedmann map itself. In particular, the duration of the geometric accelerated stage, the obstruction associated with the negative-coupling branch, and the domain of validity of the cubic truncation can all be understood directly from the function $F(H)$.

3.1. Non-Invertibility

In the reduced Planck units adopted above, the modified Friedmann equation for the cubic truncation can be written schematically as

$$3F(H) = \rho_{\rm tot}, \tag{19}$$

with

$$F(H) = H^2(1 + 16\beta H^4). \tag{20}$$

It is convenient to separate the magnitude and the sign of the cubic coupling. Since the higher-curvature corrections enter the cosmological equations through the combinations $16\beta H^4$ and $48\beta H^4$, we define

$$b \equiv 16|\beta| \geq 0, \qquad s \equiv \mathrm{sgn}(\beta) \in \{+1, -1\}, \tag{21}$$

so that $16\beta H^4 = s\, bH^4$ and $48\beta H^4 = 3s\, bH^4$. The parameter b fixes the curvature scale at which the cubic sector becomes relevant, $bH^4 \sim 1$, while the sign s controls the physical branch and the global structure of the flow. Then,

$$F(H) = H^2(1 + s\, bH^4).$$

The branch $s = +1$ corresponds to a positive cubic contribution, while $s = -1$ corresponds to the negative-coupling branch.

In General Relativity (GR), Equation (19) reduces to $\rho = 3H^2$, which is monotonic for an expanding Universe and therefore defines a locally invertible map between H and ρ. In the cubic theory, instead,

$$\frac{d\rho}{dH} = 3F_{,H} = 6H\Big(1 + 3s\, bH^4\Big). \tag{22}$$

For the positive-coupling branch $s = +1$, this derivative remains positive for $H > 0$. For the negative-coupling branch $s = -1$, however, it vanishes when

$$bH^4 = \frac{1}{3}. \tag{23}$$

This point is an extremum of $F(H)$, $F_{,H} = 0$, and therefore the inverse map $H(\rho)$ ceases to be locally well defined.

Equivalently, since the evolution equation for H follows from differentiating Equation (19),

$$3F_{,H}\dot{H} = \dot{\rho}_{\rm tot}, \tag{24}$$

and using the conservation equation, one obtains

$$\dot{H} = -\frac{\rho + p}{2(1 + 3sbH^4)}. \tag{25}$$

Thus, in the negative-coupling branch, the surface $bH^4 = 1/3$ is a branch-separating degeneracy rather than an ordinary point through which a regular cosmological solution can generically pass. If $\rho + p \neq 0$, Equation (25) implies that $\dot{H}$ diverges as this surface is approached. In the exceptional case in which $\rho + p$ vanishes simultaneously, the equation instead loses its ability to determine $\dot{H}$; this does not restore the local invertibility of the Friedmann map or define a unique regular crossing. By contrast, for $s = +1$, the factor $1 + 3bH^4$ remains strictly positive. This distinction will be important when defining the physical phase space of the dynamical system.

3.2. The Horizon Problem

A second aspect is the duration of the geometric accelerated stage. Let us first consider the scalar-free radiation-dominated regime in the positive cubic branch. In this case,

$$3\Big(H^2 + bH^6\Big) = \rho_r, \qquad \dot{\rho}_r + 4H\rho_r = 0. \tag{26}$$

Equivalently,

$$\rho_r(N) = \rho_{r,0}e^{-4N}, \qquad N \equiv \ln\left(\frac{a}{a_0}\right). \tag{27}$$

The relative strength of the cubic correction with respect to the Einstein–Hilbert term is measured by

$$B \equiv bH^4. \tag{28}$$

In the scalar-free case, using Equation (24) and radiation-conservation Equation (14) gives

$$3F_{,H}\dot{H} = \dot{\rho}_r = -4H\rho_r = -12HF(H). \tag{29}$$

Introducing the dimensionless quantity Q, which measures the fractional variation of the Hubble rate per e-fold, one obtains

$$\dot{H} = -\frac{4HF(H)}{F_{,H}}, \qquad Q \equiv \frac{\dot{H}}{H^2} = -\frac{4F(H)}{HF_{,H}}. \tag{30}$$

The condition for accelerated expansion is $Q > -1$, consistent with the corresponding relation discussed in Ref. [20].

For the positive cubic branch, $F(H) = H^2(1 + B)$, and therefore

$$Q = -\frac{2(1+B)}{1+3B}. \tag{31}$$

The condition $Q > -1$ is then equivalent to

$$\frac{2(1+B)}{1+3B} < 1 \qquad \Longleftrightarrow \qquad B > 1. \tag{32}$$

Thus, the cubic geometric sector produces accelerated expansion only while $bH^4 > 1$.

A useful way of estimating the duration of this geometric stage is to work directly with B. Without dropping the Einstein–Hilbert contribution, Equation (26) gives

$$\rho_r = 3H^2(1 + B) = 3b^{-1/2}B^{1/2}(1 + B).$$

Combining this exact relation with $\rho_r \propto e^{-4N}$ yields

$$e^{-4N} = \frac{B^{1/2}(1+B)}{B_0^{1/2}(1+B_0)}. \tag{33}$$

Setting $B = 1$ at the end of the accelerated stage yields

$$N_{\rm geo} = \frac{1}{4}\ln\left[\frac{B_0^{1/2}(1+B_0)}{2}\right]. \tag{34}$$

For $B_0 \gg 1$,

$$N_{\rm geo} = \frac{3}{8}\ln B_0 - \frac{1}{4}\ln 2 + \mathcal{O}(B_0^{-1}). \tag{35}$$

Thus, the leading behavior is logarithmic, $N_{\rm geo} = \mathcal{O}(\ln B_0)$. This is the important physical point: the cubic sector can trigger acceleration, but its duration grows only logarithmically with the initial high-curvature hierarchy.

For example, obtaining approximately 60 geometrically driven e-folds would require, at leading logarithmic order, an initial hierarchy of order

$$B_0 \sim e^{160}. \tag{36}$$

Therefore, within the cubic truncation, the geometrically accelerated stage is not long enough to solve the horizon problem for any moderate initial high-curvature hierarchy.

An important related issue is the domain of validity of the cubic truncation. Geometric acceleration requires $bH^4 > 1$, while the asymptotic high-curvature approximation corresponds to $bH^4 \gg 1$, precisely where the cubic correction dominates over the Einstein–Hilbert term. If the cubic theory is interpreted as the first non-trivial truncation of a complete higher-curvature tower, this regime cannot automatically be regarded as a controlled ultraviolet approximation, because higher-order curvature terms may also become

dynamically relevant. Thus, the cubic theory should be interpreted here as a minimal dynamical benchmark rather than as a complete high-curvature description.

The logarithmic scaling in Equation (35), the branch obstruction in Equation (23), and the need to establish anisotropic and perturbative stability [29] further show that a homogeneous cubic background analysis alone is not sufficient to establish full physical viability. The phase-space analysis remains useful for classifying homogeneous cosmological regimes, but a complete assessment also requires control of scalar, tensor, and anisotropic perturbations.

3.3. The General $F(H)$

The preceding discussion is not restricted to the cubic truncation. Consider the general relation in Equation (30),

$$Q = \frac{\dot{H}}{H^2} = -\frac{4F(H)}{HF_{,H}(H)}. \tag{37}$$

On a regular expanding branch with $F(H) > 0$ and $F_{,H}(H) > 0$, accelerated expansion requires $Q > -1$, which is equivalent to

$$4F(H) < HF_{,H}(H). \tag{38}$$

Using

$$\frac{d\ln F}{d\ln H} = \frac{HF_{,H}}{F}, \tag{39}$$

this condition can be written as

$$Q = -\frac{4}{d\ln F/d\ln H}, \qquad \frac{d\ln F}{d\ln H} > 4. \tag{40}$$

Thus, geometric acceleration is controlled not only by the magnitude of $F(H)$, but also by its logarithmic slope.

If the high-curvature behavior of the theory is approximately monomial,

$$F(H) \simeq AH^m, \qquad A > 0, \tag{41}$$

then

$$Q \simeq -\frac{4}{m}, \tag{42}$$

and such a branch accelerates only if $m > 4$. For the cubic truncation, $m = 6$, and therefore

$$Q \simeq -\frac{2}{3}. \tag{43}$$

This gives acceleration, but not a quasi-de Sitter regime.

The duration of a monomial high-curvature stage also scales logarithmically with the initial hierarchy. If

$$F(H) = H^2 + AH^m, \qquad m > 2, \tag{44}$$

and one defines the ratio

$$R \equiv AH^{m-2}, \tag{45}$$

then in the high-curvature regime $R \gg 1$,

$$\rho_r \simeq 3AH^m \quad \Rightarrow \quad R \propto \rho_r^{(m-2)/m}. \tag{46}$$

Since $\rho_r \propto e^{-4N}$,

$$R(N) = R_0 \exp\left[-\frac{4(m-2)}{m}N\right]. \tag{47}$$

For the simple form in Equation (44), the exact acceleration condition is

$$R > R_c, \qquad R_c = \frac{2}{m-4}, \qquad m > 4. \tag{48}$$

Therefore, within the high-curvature approximation, the duration of the accelerated stage is

$$N_{\rm geo} \simeq \frac{m}{4(m-2)} \ln\left(\frac{R_0}{R_c}\right). \tag{49}$$

For $m = 6$, one has $R_c = 1$, and this reduces to

$$N_{\rm geo} \simeq \frac{3}{8} \ln R_0,$$

which reproduces the leading cubic result.

Finally, any non-monotonic function $F(H)$ generically contains points satisfying

$$F_{,H}(H_\star) = 0. \tag{50}$$

At such points,

$$\left.\frac{d\rho}{dH}\right|_{H_\star} = 0, \tag{51}$$

so the map $H \mapsto \rho = 3F(H)$ ceases to be locally invertible.

Such extrema can therefore define branch boundaries or dynamical degeneracy surfaces for the background evolution. Even when the numerator of the corresponding evolution equation vanishes simultaneously, the loss of local invertibility remains, and a unique regular crossing is not guaranteed.

Consequently, a viable geometric-inflation model based on a general $F(H)$ should satisfy several basic requirements: (i) the accelerated branch must possess a sufficiently steep logarithmic dependence, $d\ln F/d\ln H > 4$, or some alternative mechanism capable of generating a quasi-de Sitter stage; (ii) the duration of acceleration must be sufficient to address the horizon problem; (iii) the relevant physical branch should avoid degeneracy surfaces with $F_{,H} = 0$, unless an additional matching or completion mechanism is supplied; (iv) the high-curvature regime must remain within the domain of validity of the effective description; and (v) the accelerated FLRW backgrounds must also be stable against scalar, tensor, and anisotropic perturbations.

These conditions provide the criteria against which we interpret the full dynamical system with radiation and a minimally coupled scalar field in the following sections.

4. Autonomous System and Phase-Space Formulation

To perform the dynamical analysis, and taking into account the analytic results of Section 3, we introduce the compactified Hubble variable

$$x \equiv \frac{bH^4}{1+bH^4} \qquad \Longleftrightarrow \qquad bH^4 = \frac{x}{1-x}, \tag{52}$$

which maps the finite expanding Hubble sector into $0 \le x < 1$. The boundary $x = 1$ is added as an asymptotic high-curvature boundary and corresponds to $H \to \infty$, whereas $x \to 0$ corresponds to the low-curvature regime $H \to 0$.

We complement this choice with the standard scalar-field variables

$$u \equiv \frac{\dot{\phi}}{\sqrt{6}\,H}, \qquad z \equiv \frac{\sqrt{V}}{\sqrt{3}\,H}, \qquad z \geq 0, \tag{53}$$

so that the scalar-field contribution satisfies $\Omega_\phi \equiv \rho_\phi/(3H^2) = u^2 + z^2$. In the phase-space formulation, we work in reduced Planck units, $\kappa^2 = 1$.

We also introduce the usual dimensionless density parameters,

$$\Omega_r \equiv \frac{\rho_r}{3H^2}, \qquad \Omega_\phi \equiv \frac{\rho_\phi}{3H^2} = u^2 + z^2, \qquad \Omega_{GI3} \equiv \frac{\rho_{GI3}}{3H^2} = -s\,bH^4 = -\frac{s\,x}{1-x}, \tag{54}$$

where in the last equalities we used $b = 16|\beta|$ and Equation (52).

The first Friedmann equation becomes the algebraic constraint

$$1 = \Omega_r + \Omega_\phi + \Omega_{GI3}, \qquad \Longrightarrow \qquad \Omega_r = 1 - (u^2 + z^2) + \frac{s\,x}{1-x}. \tag{55}$$

Accordingly, the physical region of phase space is selected by

$$0 \leq x < 1, \qquad z \geq 0, \qquad \Omega_r \geq 0, \tag{56}$$

which is equivalently expressed as the bound

$$u^2 + z^2 \leq 1 + \frac{s\,x}{1-x}. \tag{57}$$

The condition $\Omega_r \geq 0$ further restricts the admissible region depending on sign s. For $s = +1$, Equation (57) becomes

$$u^2 + z^2 \leq \frac{1}{1-x}, \tag{58}$$

and therefore the allowed domain in the (u, z) plane becomes unbounded as $x \to 1^-$. The physical phase space of the positive branch is thus

$$\Psi_+ = \left\{ (x, u, z) : z \geq 0,\ 0 \leq x < 1,\ u^2 + z^2 \leq \frac{1}{1-x} \right\}. \tag{59}$$

Consequently, although the Hubble variable is compactified, the complete $s = +1$ phase space is not globally compact. This motivates the asymptotic analysis of Section 4.1. For $s = -1$, Equation (57) instead gives

$$u^2 + z^2 \leq \frac{1-2x}{1-x}, \qquad 0 \leq x \leq \frac{1}{2}, \tag{60}$$

or, equivalently,

$$\Psi_- = \left\{ (x, u, z) : z \geq 0,\ u^2 + z^2 \leq 1,\ 0 \leq x \leq \frac{1-u^2-z^2}{2-u^2-z^2} \right\}. \tag{61}$$

This is the algebraically admissible domain. However, as shown in Section 3, the surface $x = 1/4$ is a dynamical degeneracy of the negative-coupling branch. The regular flow is therefore split into two disconnected regions separated by $x = 1/4$.

As introduced in Section 3, we define

$$Q \equiv \frac{\dot{H}}{H^2} = \frac{d \ln H}{d\eta}. \tag{62}$$

Its sign and magnitude provide a direct kinematical characterization of the cosmological evolution. In terms of Q, the deceleration parameter and the effective equation-of-state parameter are

$$q = -1 - Q, \qquad w_{\rm eff} = -1 - \frac{2}{3}Q, \tag{63}$$

so that acceleration ($\ddot{a} > 0$) corresponds to $q < 0$, i.e., $Q > -1$.

Using Equation (13), the Raychaudhuri equation, together with $p_r = \omega_r \rho_r$ with $\omega_r = 1/3$, $\rho_\phi + p_\phi = \dot{\phi}^2$, and Constraint (55) to eliminate Ω_r, one obtains an explicit expression for Q in terms of the phase-space variables (x, u, z):

$$Q = -\left[\frac{(1-x)(u^2 - 2z^2) + 2(1 - x + sx)}{1 - x + 3sx}\right]. \tag{64}$$

Equation (64) closes the system by expressing the Hubble-flow parameter purely in terms of phase-space variables, and it will be used below to write the evolution equations as an autonomous dynamical system in the e-fold time $\eta = \ln a$.

We recast the cosmological equations into an autonomous dynamical system by using the number of e-folds,

$$\eta \equiv \ln a, \qquad \frac{d}{d\eta} = \frac{1}{H}\frac{d}{dt}, \tag{65}$$

as the independent variable. In terms of the compactified Hubble variable $x = bH^4/(1 + bH^4)$ and the standard scalar-field variables $u = \dot{\phi}/(\sqrt{6}\,H)$ and $z = \sqrt{V}/(\sqrt{3}\,H)$, the evolution equations become

$$x' \equiv \frac{dx}{d\eta} = 4x(1-x)\,Q, \tag{66}$$

$$u' \equiv \frac{du}{d\eta} = -3u - uQ + \gamma z^2\sqrt{\frac{3}{2}}, \tag{67}$$

$$z' \equiv \frac{dz}{d\eta} = -zQ - \gamma uz\sqrt{\frac{3}{2}}, \tag{68}$$

Here,

$$\gamma \equiv -\frac{V_{,\phi}}{V}, \tag{69}$$

is the constant dimensionless logarithmic slope of the exponential potential $V(\phi) = V_0 e^{-\gamma\phi}$. Consequently, Equations (66)–(68) form an autonomous system of ordinary differential equations. For $s = -1$, the expression for Q in Equation (64) contains the factor $(1 - x + 3sx)^{-1}$, which becomes singular at $x = 1/4$. As shown analytically in Section 3, this corresponds to the finite value $bH^4 = 1/3$, where $F_{,H} = 0$ and the modified Friedmann map ceases to be locally invertible. The surface therefore represents a finite-H dynamical degeneracy that interrupts the regular flow and separates the negative-coupling phase space into two disconnected branches. It is not a coordinate artifact of the variable x, and a change of phase-space coordinates cannot generate a unique regular cosmological evolution across it.

Since the solutions relevant for the scenarios discussed below remain within the regular domain, we keep the variables (x, u, z) for definiteness and to facilitate comparison with the phase-space analysis.

The parameter γ controls the contribution of the potential gradient to the evolution of the scalar kinetic and potential variables. In particular, the term $+\gamma z^2\sqrt{3/2}$ in Equation (67) transfers potential contribution into the kinetic variable, whereas $-\gamma uz\sqrt{3/2}$ in Equation (68) determines the corresponding evolution of z. For $\gamma = 0$, these direct potential-gradient terms vanish, although u and z remain indirectly coupled through

$Q(x, u, z; s)$. For $\gamma \neq 0$, the potential slope shifts the location of the fixed points and may modify their stability, thereby affecting the sequence of effective cosmological regimes encoded in Q.

4.1. Asymptotic Structure of the Non-Compact $s = +1$ Branch

For $s = +1$, the physical phase space is not globally compact. Indeed, the condition $\Omega_r \geq 0$ implies

$$u^2 + z^2 \leq \frac{1}{1-x}, \tag{70}$$

so that the scalar-field variables may become unbounded in the high-curvature limit $x \to 1^-$. Therefore, in addition to the finite critical points discussed below, it is useful to examine the leading asymptotic behavior of the system as $u^2 + z^2 \to \infty$.

To this end, we introduce polar variables in the scalar-field sector,

$$R \equiv \sqrt{u^2 + z^2}, \qquad u = R\cos\theta, \qquad z = R\sin\theta, \tag{71}$$

together with the bounded combination

$$Y \equiv (1-x)R^2. \tag{72}$$

Here, R is the radial magnitude in the (u, z) subspace and therefore measures the distance from the origin in this sector of phase space, while the angular variable θ specifies the relative contribution of u and z through $u/R = \cos\theta$ and $z/R = \sin\theta$. The variable $Y = (1-x)R^2$ is a rescaled radial quantity adapted to the non-compact limit $x \to 1^-$. Since the physical constraint implies $R^2 \leq (1-x)^{-1}$, one has $0 \leq Y \leq 1$, so that Y remains bounded even when $R \to \infty$. In this sense, Y measures the radial position relative to the maximal value allowed by the physical phase-space constraint.

From Equation (70), the physical region satisfies

$$0 \leq Y \leq 1. \tag{73}$$

Notice that $R \to \infty$ can therefore occur only simultaneously with $x \to 1^-$.

For $s = +1$, Equation (64) can be written exactly as

$$Q = -\frac{Y\left(1 - 3\sin^2\theta\right) + 2}{1 + 2x}. \tag{74}$$

Using Equations (66)–(68), the evolution equations for R, θ, and Y take the form

$$\frac{R'}{R} = -3\cos^2\theta - Q, \tag{75}$$

$$\theta' = \sin\theta\left(3\cos\theta - \gamma\sqrt{\frac{3}{2}}\,R\right), \tag{76}$$

$$Y' = 2Y(1-Y)\left(3\sin^2\theta - 1\right). \tag{77}$$

These relations provide a direct characterization of the non-compact boundary without assuming that the finite (u, z) chart exhausts the global phase-space structure. It is worth noting that the change of variables becomes singular at $(u^2 + z^2 = 0)$, i.e., at (R = 0), where the angular variable θ is not defined. This is, however, only a coordinate singularity introduced by the polar parametrization. The original dynamical system written in terms of u and z remains regular at this point.

For $\gamma \neq 0$, Equation (76) shows that, in the limit $R \to \infty$, any asymptotically stationary direction must approach

$$\sin\theta \to 0, \tag{78}$$

unless the angular variable evolves without approaching a limiting direction. Hence, the candidate stationary directions at infinity are kinetic-dominated,

$$\frac{z}{R} \to 0, \qquad \frac{u}{R} \to \pm 1. \tag{79}$$

Along these directions, taking $x \to 1^-$ gives

$$Q_\infty = -\frac{Y+2}{3}, \qquad \frac{R'}{R} = \frac{Y-7}{3}, \qquad 0 \leq Y \leq 1. \tag{80}$$

Since

$$\frac{Y-7}{3} < 0 \tag{81}$$

throughout the physical interval, sufficiently large values of R decrease toward the future along these kinetic-dominated asymptotic directions. They therefore do not behave as additional future radial attractors.

The corresponding first Hubble-flow parameter, $\epsilon_1 \equiv -Q$ (introduced systematically in Section 4.3), and the deceleration parameter are

$$\epsilon_{1,\infty} = -Q_\infty = \frac{Y+2}{3}, \qquad q_\infty = -1 - Q_\infty = \frac{Y-1}{3}, \tag{82}$$

and consequently

$$\frac{2}{3} \leq \epsilon_{1,\infty} \leq 1, \qquad -\frac{1}{3} \leq q_\infty \leq 0. \tag{83}$$

Thus, weak accelerated expansion is possible for $Y < 1$, but $\epsilon_{1,\infty} \geq 2/3$; hence this asymptotic sector is far from quasi-de Sitter slow roll and does not provide an additional inflationary future attractor. In particular, along these directions, Equation (77) becomes

$$Y' = -2Y(1-Y), \tag{84}$$

so that for $0 < Y < 1$ the backward asymptotic evolution tends toward $Y \to 1$, for which $\epsilon_1 \to 1$ and $q \to 0$.

The case $\gamma = 0$ deserves separate consideration. Equation (76) then reduces to

$$\theta' = 3\sin\theta\cos\theta. \tag{85}$$

Besides the kinetic directions, the potential-dominated direction $\theta = \pi/2$ becomes possible. For

$$\theta = \frac{\pi}{2}, \qquad Y = 1, \tag{86}$$

one has

$$u = 0, \qquad z^2 = \frac{1}{1-x}, \qquad Q = 0, \tag{87}$$

and therefore

$$x' = u' = z' = 0. \tag{88}$$

This is precisely the one-dimensional de Sitter critical manifold present when the potential is constant. Its $s = +1$ branch extends continuously toward

$$x \to 1^-, \qquad z \to \infty, \tag{89}$$

showing explicitly that the de Sitter family extends asymptotically into the non-compact (u, z) sector.

The above analysis does not constitute a full Poincaré compactification of the three-dimensional system and is therefore not intended as an exhaustive topological classification of its boundary at infinity. It nevertheless shows that, for $\gamma \neq 0$, the candidate stationary directions associated with $R \to \infty$ are kinetic dominated and do not generate an additional quasi-de Sitter future attractor. For $\gamma = 0$, the non-compact boundary instead contains the asymptotic continuation of the de Sitter critical manifold. Accordingly, the finite critical points discussed below should be interpreted as the complete set of finite equilibria, while the present asymptotic analysis specifies the relevant behavior of the non-compact $s = +1$ sector.

4.2. Effective-Fluid Diagnostics of the Cosmological Background

Since the present work is restricted to homogeneous FLRW dynamics, the standard energy conditions are used only as kinematical diagnostics of the effective background evolution. They should not be interpreted as fundamental stability or viability conditions for the higher-curvature theory. A genuine stability analysis would require the scalar and tensor perturbation sectors, including their kinetic coefficients and propagation speeds. Writing the modified Friedmann equations in effective-fluid form,

$$\rho_{\rm eff} \equiv \rho + \rho_{\rm GI3}, \qquad p_{\rm eff} \equiv p + p_{\rm GI3}, \tag{90}$$

and using reduced Planck units, the flat-FLRW equations give

$$\rho_{\rm eff} = 3H^2, \qquad \rho_{\rm eff} + p_{\rm eff} = -2QH^2, \qquad \rho_{\rm eff} + 3p_{\rm eff} = -6(1+Q)H^2. \tag{91}$$

We use the null energy condition (NEC), weak energy condition (WEC), strong energy condition (SEC), and dominant energy condition (DEC) only to characterize the corresponding effective FLRW regimes. Their equivalent conditions in terms of Q are summarized in Table 1.

Table 1. Energy conditions applied to the effective FLRW fluid and their kinematical expressions in terms of $Q = \dot{H}/H^2$. These relations are used only as background diagnostics and not as perturbative stability criteria.

Condition	Standard Form (Effective Fluid)	Equivalent Condition
NEC	$\rho_{\rm eff} + p_{\rm eff} \geq 0$	$Q \leq 0$
WEC	$\rho_{\rm eff} \geq 0$ and $\rho_{\rm eff} + p_{\rm eff} \geq 0$	$Q \leq 0$
SEC	$\rho_{\rm eff} + 3p_{\rm eff} \geq 0$ and $\rho_{\rm eff} + p_{\rm eff} \geq 0$	$Q \leq -1$
DEC	$\rho_{\rm eff} \geq 0$ and $\rho_{\rm eff} \pm p_{\rm eff} \geq 0$	$-3 \leq Q \leq 0$

Accelerated expansion corresponds to

$$q < 0 \iff Q > -1 \iff w_{\rm eff} < -\frac{1}{3}, \tag{92}$$

and therefore violates the effective SEC. Effective NEC violation corresponds to $Q > 0$ and describes a super-accelerating or phantom-like background. These relations will be used below only to characterize the critical points and representative trajectories.

4.3. Hubble-Flow Parameters and Inflationary Diagnostics

To quantify the quasi-de Sitter character of the inflationary stage and to facilitate contact with CMB-oriented parametrizations, we use the first two Hubble-flow

parameters [31,32], widely employed as background diagnostics and previously applied in geometric-inflation scenarios [26]. Since the background evolution is formulated in terms of the e-folding time $\eta \equiv \ln a$, we define

$$\epsilon_1 \equiv -\frac{\dot{H}}{H^2} = -Q, \qquad \epsilon_2 \equiv \frac{d\ln|\epsilon_1|}{d\eta}. \tag{93}$$

Inflation, $\ddot{a} > 0$, corresponds to $\epsilon_1 < 1$, while a quasi-de Sitter regime is characterized by $0 < \epsilon_1 \ll 1$. Using Equation (64), the first parameter reads explicitly

$$\epsilon_1(x,u,z;s) = \frac{(1-x)(u^2-2z^2)+2(1-x+sx)}{1-x+3sx}. \tag{94}$$

For this analysis, we need only the second Hubble-flow parameter. It is obtained directly by differentiating ϵ_1 along the autonomous flow,

$$\epsilon_2 = \frac{d\ln|\epsilon_1|}{d\eta} = \frac{1}{\epsilon_1}\frac{d\epsilon_1}{d\eta}, \qquad \frac{d\epsilon_1}{d\eta} = \frac{\partial\epsilon_1}{\partial x}x' + \frac{\partial\epsilon_1}{\partial u}u' + \frac{\partial\epsilon_1}{\partial z}z'. \tag{95}$$

Thus, ϵ_1 is an algebraic function of the phase-space variables, whereas ϵ_2 depends on the derivative along the dynamical flow. Its fully expanded expression is lengthy and is therefore evaluated directly from the autonomous system when needed.

We now wish to determine how the strength of cubic Geometric Inflation, encoded in b, see Equation (21), and the logarithmic slope of the potential, γ, see Equation (69), affect the slow-roll parameters, with the aim of assessing whether the resulting background evolution can approach the observationally relevant inflationary regime. While γ appears explicitly in the equations of motion, b is hidden in the dynamical variable x, so it is useful to introduce a reparametrization that makes its role more explicit.

As defined in Section 3, the instantaneous relative strength of the cubic correction is $B = bH^4$. For the numerical trajectories, its initial value is

$$B_0 \equiv bH_0^4, \qquad x_0 = \frac{B_0}{1+B_0}. \tag{96}$$

Thus, $B_0 \in [0,\infty)$, with $B_0 = 0 \leftrightarrow x_0 = 0$ and $B_0 \to \infty \leftrightarrow x_0 \to 1$. For consistency with the notation used in the numerical figures, the initial parameter B_0 is denoted simply by B in the figure labels. It should therefore be understood there as a parametrization of the initial strength of the cubic sector rather than as an additional independent dynamical parameter.

With this parametrization, we compute the inflationary diagnostic quantities considered in this work. As shown analytically in Section 3 and further supported by the critical-point analysis of Section 5, the numerical trajectories are used here primarily to illustrate the resulting background dynamics. For the inflationary diagnostic, we work consistently at first order in the standard GR-based Hubble-flow mapping and retain only the quantities actually used in the analysis:

$$n_s \simeq 1 - 2\epsilon_1 - \epsilon_2, \tag{97}$$

$$r \simeq 16\epsilon_1. \tag{98}$$

Here, n_s is the scalar spectral index, which characterizes the scale dependence of the primordial scalar spectrum, while r is the tensor-to-scalar ratio. We emphasize that Equations (97) and (98) are employed only as standard GR-based background diagnostics. They are not a substitute for a derivation of the scalar and tensor perturbation spectra in the cubic higher-curvature theory. Accordingly, we use ϵ_1 and ϵ_2 to characterize the

background slow-roll behavior and n_s and r only to assess whether the corresponding GR-based diagnostic approaches the observationally relevant region. A definitive comparison with CMB data would require the full perturbation analysis.

As emphasized in the Introduction, these expressions are used only as background-level GR-based diagnostics. The numerical trajectories will therefore be used to illustrate the evolution of ϵ_1 and ϵ_2 and the corresponding behavior of n_s and r. As shown below, the critical-point analysis provides the analytic explanation of the resulting observational tension, so the numerical exploration of (B, γ) should be understood as illustrative rather than as the basis for the general conclusion.

5. Analysis of the Model

5.1. Critical Points, Phase-Space Structure, and Energy Conditions

The $s = -1$ branch is dynamically obstructed by the singular surface $x = 1/4$, and therefore it cannot be interpreted as a globally regular cosmological trajectory. Nevertheless, its fixed-point structure remains informative. In particular, the critical points of this branch describe formal asymptotic regimes of the high-curvature sector and help us understand how the geometric contribution may drive, mimic, or obstruct an initial accelerated phase. For this reason, we analyze the $s = -1$ critical points as part of the mathematical phase-space classification, while excluding this branch as a viable global cosmological evolution.

The critical points and the corresponding dynamics depend on the sign s of β and on the parameter γ. The sign s selects the relevant geometric branch of the phase space, while γ determines the scalar-field trajectory within it. We now analyze the critical points $P_i : (x_i, u_i, z_i)$ that result from the autonomous system defined by Equations (66)–(68), together with their energy conditions and the constraint equation that determines the physical phase space, Ψ.

We can group them into three classes. The first class corresponds to geometric-dominated configurations, represented by the boundary point P_{gw} and $P_{g\phi}$ for $s = +1$ and by the finite-curvature point P_{gdS} for $s = -1$. The second class contains the standard radiation and kinetic-scalar solutions, P_r and P_k, which describe decelerated regimes. The third class contains scalar-field-dominated and radiation-scalar scaling solutions, $P_{\rm SF}$ and $P_{\rm SS}$, as well as the de Sitter point $P_{\rm dS}$ for $\gamma = 0$. The critical points of the autonomous system are summarized in Table 2. Here we list only the physically relevant properties: existence, effective regime, deceleration parameter, and stability character.

- **Geometric weak-acceleration point**, $P_{gw}(1, 0, 0)$: $\Omega_\phi = 0$. This point lies at the edge of the phase space because, as $x \to 1$, $H \to \infty$, corresponding to an ultra-curvature regime in the $s = +1$ branch. Using the Friedmann constraint (55), one finds that the term $x/(1-x)$ diverges as $x \to 1$, while Ω_ϕ remains finite for fixed γ; hence, $\Omega_r \to \infty$. It has $q = -1/3$ and $\omega_{\rm eff} = -5/9$, and therefore represents a weakly accelerated geometric regime. The eigenvalues are $\lambda_u = -7/3$, $\lambda_z = 2/3$, and $\lambda_x = 8/3$, which show that it is a saddle point. Hence, it can act as a transient high-curvature stage, but not as a stable past attractor. At this point, NEC, WEC, and DEC are satisfied, whereas SEC is violated, consistent with the solution's accelerated character. More precisely, P_{gw} lies on the asymptotic boundary $x = 1$ of the $s = +1$ branch. Since $x = 1$ corresponds to $H \to \infty$, it should be interpreted as an asymptotic boundary configuration rather than as a finite-H point of Ψ_+.
- **Geometric scalar point**, $P_{g\phi}(1, \frac{2\sqrt{6}}{9\gamma}, \frac{2\sqrt{7}}{3\sqrt{3}|\gamma|})$: This point appears in the $s = 1$ branch at $x = 1$, i.e., in the limit $H \to \infty$. It corresponds to an asymptotic high-curvature state in which the cubic geometric sector and the scalar field are simultaneously active. Using the Friedmann constraint (55), one finds that $x/(1-x)$ diverges as $x \to 1$, while Ω_ϕ

remains finite for fixed γ; hence, $\Omega_r \to \infty$. With $q = -1/3$ and $\omega_{\rm eff} = -5/9$, this point also represents a weakly accelerated regime. The eigenvalues are $(8/3, -7/6 + (i\sqrt{7}/2), -7/6 - (i\sqrt{7}/2))$, which correspond, at the linearized level, to a spiral saddle point. NEC, WEC, and DEC are satisfied, while SEC is violated, in agreement with the deceleration parameter. Both positive-branch high-curvature points, P_{gw} and $P_{g\phi}$, share the values $q = -1/3$, $\omega_{\rm eff} = -5/9$, and $\epsilon_1 = 2/3$. They therefore represent genuinely accelerated configurations, but not quasi-de Sitter states. Their acceleration is of the weak power-law type and cannot, by itself, reproduce a conventional slow-roll stage. More precisely, $P_{g\phi}$ lies on the asymptotic boundary $x = 1$ of the $s = +1$ branch. Since $x = 1$ corresponds to $H \to \infty$, it should be interpreted as an asymptotic boundary configuration rather than as a finite-H point of Ψ_+.

- **Geometric de Sitter point**, $P_{gdS}(\frac{1}{2}, 0, 0)$: Although this point appears formally in the $s = -1$ branch at $x = 1/2$, its physical interpretation must be treated with care. It behaves as a finite-curvature de Sitter-like point. For this branch, $\Omega_\phi = 0$, and since H does not reach infinity, one has $\Omega_r = 0$. This point has $q = -1$ and $\omega_{\rm eff} = -1$. The eigenvalues are $\lambda_z = 0$, $\lambda_u = -3$, and $\lambda_x = -4$. It should not be interpreted as a physical partial past attractor accessible from ordinary initial conditions. Rather, it reveals the bounded algebraic structure of the negative branch. Its classification depends on the value of γ. For $\gamma \neq 0$, P_{gdS} remains an isolated non-hyperbolic equilibrium. A centre-manifold analysis, presented below, shows that it is stable along the centre direction. For $\gamma = 0$, however, the situation changes qualitatively because the potential becomes constant. In this case, P_{gdS} belongs to the one-dimensional de Sitter critical manifold

$$\mathcal{C}_- : \qquad u = 0, \qquad z^2 = \frac{1-2x}{1-x}.$$

Along the regular portions of this curve, one has $\Omega_r = 0$, $Q = 0$, and $x' = u' = z' = 0$, with one tangent zero eigenvalue and transverse eigenvalues -3 and -4. The degenerate surface $x = 1/4$ divides this algebraic de Sitter family into two dynamically disconnected regular segments,

$$\mathcal{C}_-^{\rm low} : \quad 0 \le x < \frac{1}{4}, \qquad \mathcal{C}_-^{\rm high} : \quad \frac{1}{4} < x \le \frac{1}{2}.$$

The low-curvature segment contains P_{dS} at $x = 0$, while the high-curvature segment terminates at P_{gdS} at $x = 1/2$. Although these two segments belong to the same algebraic curve, they cannot be connected by a regular cosmological trajectory because the modified Friedmann map is degenerate at $x = 1/4$. At this point, NEC, WEC, and DEC are satisfied, while SEC is violated.

- **Radiation-dominated point**, $P_r(0, 0, 0)$: $\Omega_r = 1$ and $\Omega_\phi = 0$. It has $q = 1$ and $\omega_{\rm eff} = \frac{1}{3}$, and represents the standard decelerated radiation-dominated solution. The eigenvalues are $(-8, 2, -1)$, indicating a saddle point, as expected for an intermediate cosmological phase. This point does not depend on s or on γ, at least at the linear level. All energy conditions are satisfied.
- **Kinetic scalar point**, $P_k(0, \pm 1, 0)$: $\Omega_{GI3} = 0$ and $\Omega_r = 0$. These points correspond to stiff-fluid solutions with $p_\phi \simeq \rho_\phi$, dominated by the scalar kinetic energy. They are decelerated and behave as saddle points in the physical phase space. The eigenvalues are $(-12, 2, (3 \mp \gamma\sqrt{6}/2))$. This point does not depend on s, and although it depends on γ, that does not change the fact that it remains a saddle point. All energy conditions are satisfied.

https://doi.org/10.3390/universe12100307

- **Scalar-field point**, $P_{SF}(0, \frac{\gamma}{\sqrt{6}}, \sqrt{1-\frac{\gamma^2}{6}})$: $\Omega_{GI3} = 0$ and $\Omega_r = 0$. The deceleration parameter is $q = \frac{\gamma^2}{2} - 1$ and $\omega_{\text{eff}} = \frac{\gamma^2}{3} - 1$. The eigenvalue set is $\left\{-2\gamma^2, \gamma^2 - 4, \frac{\gamma^2}{2} - 3\right\}$. For $\gamma \neq 0$, the scalar perturbation eigenmodes are in general mixtures of the u and z directions; in the limit $\gamma \to 0$, the latter two eigenvalues reduce to -4 and -3, consistent with the de Sitter limit. It is a future attractor for $0 < \gamma^2 < 4$, a saddle for $4 < \gamma^2 < 6$, and non-hyperbolic at $\gamma^2 = 0, 4, 6$. Therefore, it is accelerated when $\gamma^2 < 2$, decelerated when $2 < \gamma^2 < 6$, and lies on the acceleration boundary when $\gamma^2 = 2$. This point formally exists for $0 \leq \gamma^2 \leq 6$. The endpoints correspond to limiting cases: for $\gamma = 0$, it coincides with the de Sitter point, while for $\gamma^2 = 6$ it coincides with a kinetic-scalar solution. Since at this fixed point the first Hubble-flow parameter is constant, $\epsilon_1 = \gamma^2/2$, the scalar-field-dominated regime corresponds to a power-law solution rather than to a slow-roll regime with a dynamical exit. Thus, for $0 < \gamma^2 < 2$, P_{SF} is an eternally accelerating future attractor, while for $2 < \gamma^2 < 4$ it is a decelerated attractor with $\Omega_r = 0$ and therefore does not provide a standard radiation era. We analyze the corresponding inflationary diagnostics separately below.
- **Radiation-scalar-scaling point**, $P_{SS}(0, \frac{4}{\gamma\sqrt{6}}, \frac{2}{\gamma\sqrt{3}})$: For this point, $\Omega_{GI3} = 0$. It is a scaling solution between radiation and the scalar field. Using the first Friedmann equation, one obtains $\Omega_r = 1 - 4/\gamma^2$, so this point exists only if $\gamma^2 \geq 4$. The deceleration parameter is $q = 1$ and $\omega_{\text{eff}} = \frac{1}{3}$. The eigenvalues are

$$\lambda_x = -8, \qquad \lambda_\pm = -\frac{1}{2} \pm \frac{1}{2}\sqrt{\frac{64}{\gamma^2} - 15}.$$

  Therefore, for $\gamma^2 = 4$, one eigenvalue vanishes, and the point is non-hyperbolic. For $4 < \gamma^2 \leq 64/15$, all eigenvalues are real and negative, so the point is a node attractor. For $\gamma^2 > 64/15$, the pair $\lambda_\pm$ becomes complex with a negative real part, and the point is a spiral attractor. All energy conditions are satisfied.
- **de Sitter point**, $P_{dS}(0, 0, 1)$: this point is a special case for $\gamma = 0$, for which $V = \text{const}$. The scalar-field equation simplifies and allows $\dot{\phi} = 0$, while $\Omega_{GI3} = 0$. For $\gamma = 0$, this point should be understood as part of a continuous de Sitter critical manifold rather than as an isolated equilibrium. For the positive branch, $\mathcal{C}_+ : \quad u = 0, \quad z^2 = \frac{1}{1-x}, \quad 0 \leq x < 1$, and along this curve one has $\Omega_r = 0$, $Q = 0$, and $x' = u' = z' = 0$. The point P_{dS} corresponds to its low-curvature endpoint $x = 0$, while $\mathcal{C}_+$ extends asymptotically toward $x \to 1^-$ and $z \to \infty$. For the negative branch, the corresponding de Sitter family is $\mathcal{C}_- : \quad u = 0, \quad z^2 = \frac{1-2x}{1-x}$, whose regular portions are separated by the degeneracy at $x = 1/4$, as discussed above. In this branch, P_{dS} belongs to the low-curvature segment, whereas P_{gdS} belongs to the high-curvature segment. Thus, although both points belong algebraically to the same $\mathcal{C}_-$ curve when $\gamma = 0$, they are not connected by a regular cosmological trajectory. The transverse eigenvalues along the regular de Sitter manifolds are -3 and -4, while the vanishing eigenvalue is tangent to the critical manifold. Hence, the regular segments of the de Sitter critical manifolds are normally hyperbolic and transversely attracting. At this point, NEC, WEC, and DEC are satisfied, whereas SEC is violated, consistently with its accelerated character.

At the scalar-field-dominated fixed point P_{SF}, the first Hubble-flow parameter is constant,

$$\epsilon_1 = \frac{\gamma^2}{2},$$

and therefore, for $\gamma \neq 0$,

$$\epsilon_2 = \frac{d \ln |\epsilon_1|}{d\eta} = 0.$$

Using the first-order GR-based diagnostic relations,

$$n_s \simeq 1 - 2\epsilon_1 - \epsilon_2, \qquad r \simeq 16\epsilon_1,$$

one obtains

$$n_s \simeq 1 - \gamma^2, \qquad r \simeq 8\gamma^2,$$

and hence

$$r \simeq 8(1 - n_s). \tag{99}$$

Table 2. Critical points of the autonomous system and their main physical properties. Here, $s = \mathrm{sgn}(\beta)$, $\gamma = -V_{,\phi}/V$, q is the deceleration parameter, and ω_{eff} is the effective equation-of-state parameter. The symbols ✓ and X indicate, respectively, whether the corresponding energy condition is satisfied or violated. The configurations P_{gw} and $P_{g\phi}$ are included for completeness. They belong to the asymptotic boundary $x = 1$ of the $s = +1$ branch, corresponding to $H \to \infty$, and therefore are not finite-H points of the physical phase space Ψ_+.

Critical Point	Physical Regime	Existence	Eigenvalues	q	ω_{eff}	Type	NEC	SEC
$P_{gw}(1,0,0)$	Weak GI	$\forall\gamma, s=+1$	$\frac{8}{3}, -\frac{7}{3}, \frac{2}{3}$	$-\frac{1}{3}$	$-\frac{5}{9}$	saddle	✓	X
$P_{gdS}\left(\frac{1}{2},0,0\right)$	de Sitter GI	$\forall\gamma, s=-1$	$-4,-3,0$	-1	-1	isolated non-hyperbolic; centre-manifold stable for $\gamma \neq 0$; endpoint of normally hyperbolic $\mathcal{C}_-$ for $\gamma = 0$	✓	X
$P_{g\phi}\left(1, \frac{2\sqrt{6}}{9\gamma}, \frac{2\sqrt{7}}{3\sqrt{3}\lvert\gamma\rvert}\right)$	GI-scalar	$\gamma \neq 0, s=+1$	$\frac{8}{3}, -\frac{7}{6} \pm \frac{i\sqrt{7}}{2}$	$-\frac{1}{3}$	$-\frac{5}{9}$	spiral saddle	✓	X
$P_r(0,0,0)$	Radiation	$\forall\gamma, s$	$-8, 2, -1$	1	$\frac{1}{3}$	saddle	✓	✓
$P_k(0,\pm1,0)$	Kinetic scalar	$\forall\gamma, s$	$-12, 2, 3 \mp \frac{\gamma\sqrt{6}}{2}$	2	1	saddle	✓	✓
$P_{SF}\left(0, \frac{\gamma}{\sqrt{6}}, \sqrt{1-\frac{\gamma^2}{6}}\right)$	Scalar field	$0 \leq \gamma^2 \leq 6$	$-2\gamma^2, \gamma^2-4, \frac{\gamma^2}{2}-3$	$\frac{\gamma^2}{2}-1$	$\frac{\gamma^2}{3}-1$	future attractor: $0 < \gamma^2 < 4$ saddle: $4 < \gamma^2 < 6$ non-hyperbolic: $\gamma^2 = 0, 4, 6$	✓	X if $\gamma^2 < 2$ ✓ if $\gamma^2 \geq 2$
$P_{SS}\left(0, \frac{4}{\gamma\sqrt{6}}, \frac{2}{\gamma\sqrt{3}}\right)$	rad.- ϕ scaling	$\gamma^2 \geq 4$	$-8, \lambda_-, \lambda_+$	1	$\frac{1}{3}$	non-hyperbolic: $\gamma^2 = 4$ node attractor: $4 < \gamma^2 \leq \frac{64}{15}$ spiral attractor: $\gamma^2 > \frac{64}{15}$	✓	✓
$P_{dS}(0,0,1)$	de Sitter	$\gamma = 0$	$0, -3, -4$	-1	-1	member of normally hyperbolic de Sitter manifold	✓	X

For P_{SS}, $\lambda_\pm = -\frac{1}{2} \pm \frac{1}{2}\sqrt{\frac{64}{\gamma^2} - 15}$. We evaluate NEC and SEC for the effective fluid description. For the scalar-field point P_{SF}, SEC is violated in the accelerated range $\gamma^2 < 2$ and is satisfied for $\gamma^2 \geq 2$.

This is the standard power-law-inflation relation associated with a constant-slope exponential potential. Importantly, the cubic parameter does not enter this relation because P_{SF} lies at $x = 0$, where the cubic geometric contribution vanishes. Consequently, the late-time scalar-field diagnostic is controlled by γ rather than by the initial strength of the cubic sector. The numerical trajectories shown below are therefore used only to illustrate this analytic obstruction.

The point P_{gdS} is non-hyperbolic because one eigenvalue vanishes. Therefore, we cannot infer its stability solely from the linearized system. Introducing local coordinates around P_{gdS}, the center manifold is given, at leading order, by

$$u \simeq \frac{\gamma}{3}\sqrt{\frac{3}{2}}\, z^2.$$

The reduced dynamics along the center direction are then

$$z' \simeq -\frac{\gamma^2}{2} z^3.$$

For $\gamma \neq 0$, this term drives z toward zero within the physical domain. Hence, although P_{gdS} is non-hyperbolic at the linear level, it is stable along the centre direction. For $\gamma = 0$, the leading reduced flow vanishes, consistent with the fact that P_{gdS} becomes an endpoint of the de Sitter critical manifold $\mathcal{C}_-$.

In view of the above, we illustrate three representative trajectories, corresponding to $\gamma^2 = 0, 1$, and 4.2. For clarity, we display the $s = +1$ branch in Figure 1. The first column corresponds to $\gamma = 0$, the second to $\gamma = 1$, and the third to $\gamma^2 = 4.2$. Blue trajectories show the dynamical evolution, while red spheres mark the critical points. We also include the surface where the deceleration parameter satisfies $q = 0$, as determined from Equation (64). This implies the relation $u^2 - 2z^2 = -1 + \frac{sx}{1-x}$, which defines the boundary between accelerated and decelerated regions. For the first two columns, corresponding to $\gamma = 0$ and $\gamma = 1$, the numerical trajectories exhibit cascade-like early-universe dynamics: the Universe starts in an accelerated geometric phase, then enters a decelerating regime, and finally accelerates again due to the scalar field. For the third case, where $\gamma^2 > 4$, the trajectories end in a decelerated regime.

For completeness, we also examined representative trajectories in the $s = -1$ branch, although only as a formal diagnostic, since this branch is not globally viable. The main difference between the two branches is that $\beta > 0$ produces a weak early accelerated phase, whereas $\beta < 0$ yields an exact de Sitter-like initial stage, thereby avoiding the divergence $\Omega_r \to \infty$. This conclusion is relevant because the inclusion of a minimally coupled scalar field does not resolve the trans-Planckian radiation problem previously identified for the cubic geometric-inflation model. Hence, within the cubic truncation considered here, there is no branch that simultaneously provides a regular high-curvature evolution and a bounded early-time radiation sector. In particular, the geometric critical points P_{gw} and $P_{g\phi}$ still satisfy $\Omega_r \to \infty$, so the regular branch continues to involve a trans-Planckian radiation density in the asymptotic past. The only branch that avoids this behavior is the negative-coupling branch, $\beta < 0$, but it is dynamically singular, separated by the degeneracy of the modified Friedmann map. The failure is not necessarily a failure of Geometric Inflation, but of the cubic truncation as a complete early-time description. This obstruction suggests that curing the early-time radiation divergence may require contributions from higher-order members of the geometric-inflation tower rather than adding a minimally coupled scalar field alone.

The slope γ of the exponential potential determines the late-time cosmological regime. Table 3 summarizes the complete range of γ relevant to the fixed-point structure.

Table 3 makes explicit why the minimal exponential model does not provide a standard graceful exit for any value of γ. For $\gamma = 0$, the constant potential generates de Sitter critical manifolds and there is no dynamical exit from the accelerated state. For $0 < \gamma^2 < 2$, P_{SF} is an accelerated future attractor with $\epsilon_1 = \gamma^2/2 < 1$, so scalar-driven inflation persists asymptotically.

At $\gamma^2 = 2$, P_{SF} lies exactly on the acceleration–deceleration boundary, $\epsilon_1 = 1$ and $q = 0$. Although accelerated expansion ends kinematically at this limiting solution, P_{SF} remains a stable scalar-field-dominated state with $\Omega_r = 0$; there is therefore no graceful transition to a radiation-dominated epoch. For $2 < \gamma^2 < 4$, the same fixed point is a decelerated future attractor, again with $\Omega_r = 0$.

Table 3. Late-time dynamical regimes as a function of the exponential-potential parameter γ, together with their cosmological interpretation and dependence on the cubic coupling β. The parameter β mainly affects the high-curvature and transient dynamics, whereas the late-time scalar–radiation attractor structure is controlled primarily by γ. The late-time viability discussion focuses on the regular $s = +1$ branch, while the $s = -1$ branch is retained only for the formal phase-space classification because its regular evolution is interrupted by the finite-curvature degeneracy at $x = 1/4$.

Range of γ	Future Structure	Cosmological Consequence	Dependence on β
$\gamma = 0$	Continuous de Sitter critical line	No graceful exit. The late-time evolution approaches a de Sitter configuration.	The critical-line structure depends on $s = \mathrm{sgn}(\beta)$.
$0 < \gamma^2 < 2$	P_{SF} accelerated hyperbolic attractor	The Universe approaches an asymptotically accelerated regime, with $\epsilon_1 = \gamma^2/2 < 1$, and inflation does not end.	Asymptotically independent of β.
$\gamma^2 = 2$	P_{SF} hyperbolic attractor at the acceleration–deceleration boundary	$\epsilon_1 = 1$ and $q = 0$, corresponding to the boundary between accelerated and decelerated expansion. This is a cosmological boundary, not a loss of stability of P_{SF}.	Asymptotically independent of β.
$2 < \gamma^2 < 4$	P_{SF} decelerated hyperbolic attractor	Acceleration ends, but $\Omega_r \to 0$. Hence, no standard radiation-dominated era is reached.	Asymptotically independent of β.
$\gamma^2 = 4$	Coincidence point $P_{SF} = P_{SS}$; transition in the stability structure	The scalar-field-dominated solution joins the scalar–radiation scaling solution. In the full system, one eigenvalue associated with P_{SF} vanishes, marking the transition between the two regimes.	Asymptotically independent of β.
$4 < \gamma^2 < 6$	P_{SS} scaling attractor; P_{SF} remains physical but becomes a saddle	The scalar field tracks the radiation component. The asymptotic state is therefore a scalar–radiation scaling regime, rather than a purely radiation-dominated epoch.	Asymptotically independent of β at P_{SS}.
$\gamma^2 = 6$	P_{SS} scaling attractor; P_{SF} reaches the non-hyperbolic kinetic endpoint	P_{SF} reaches the kinetic-scalar configuration and lies on the boundary of its physical existence domain. It is not the generic future state; the late-time evolution is governed by P_{SS}.	Asymptotically independent of β.
$\gamma^2 > 6$	P_{SS} scaling attractor; P_{SF} no longer belongs to the physical phase space	P_{SF} ceases to be physically admissible. The scalar field continues to track radiation through P_{SS}. For finite γ, the final state is not exactly radiation dominated, although it approaches radiation domination as $\gamma^2 \to \infty$.	Asymptotically independent of β.

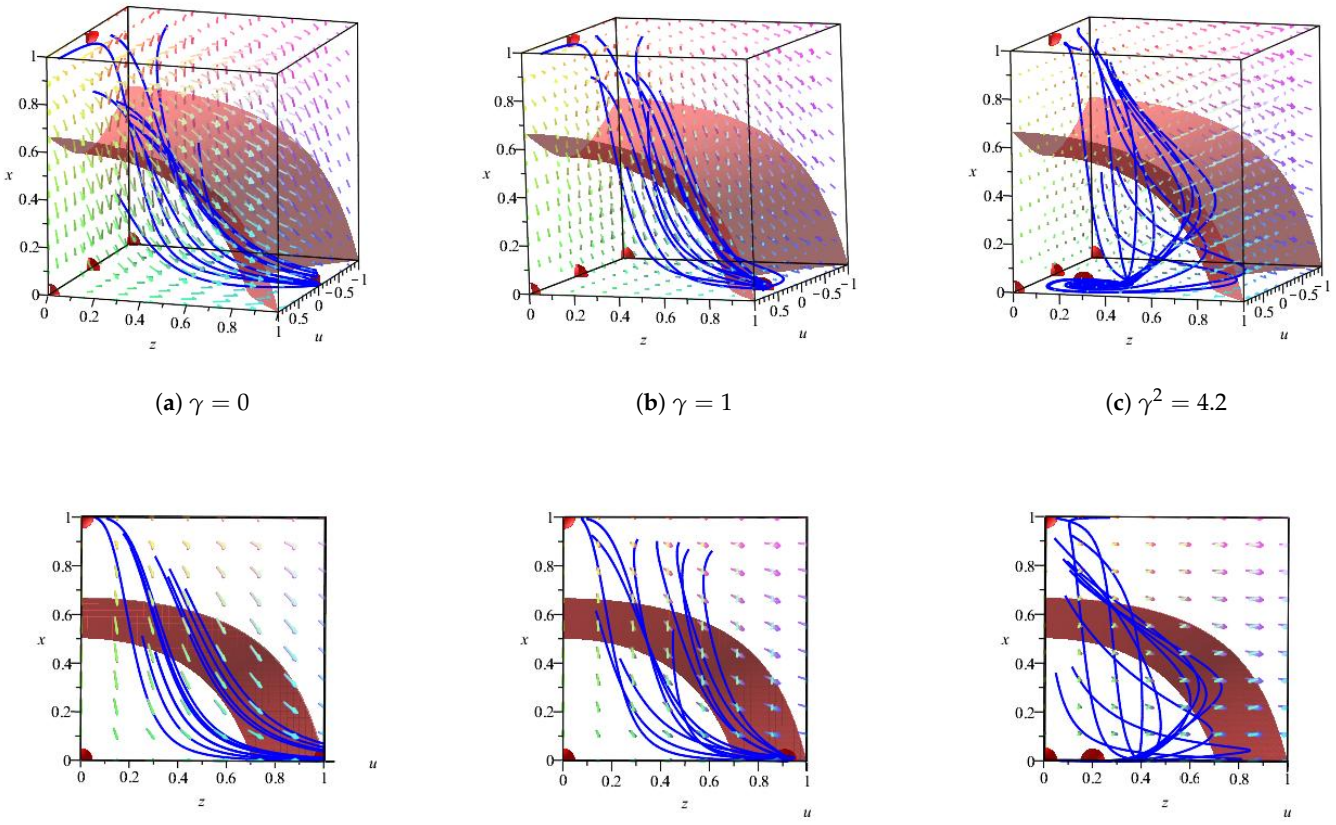
At $\gamma^2 = 4$, P_{SF} and P_{SS} coalesce into a non-hyperbolic critical point, marking the transition between scalar-field domination and scalar–radiation scaling. For $\gamma^2 > 4$, the future attractor is P_{SS}, for which

$$\omega_{\mathrm{eff}} = \frac{1}{3}, \qquad q = 1, \qquad \Omega_\phi = \frac{4}{\gamma^2}, \qquad \Omega_r = 1 - \frac{4}{\gamma^2}.$$

Thus, the total background has a radiation-like equation of state, but for any finite γ the scalar field retains a nonzero fractional density. Only in the formal limit $\gamma^2 \to \infty$ do $\Omega_\phi \to 0$ and the solution approach pure radiation domination.

At $\gamma^2 = 6$, P_{SF} reaches the kinetic-scalar boundary of its physical existence domain, while P_{SS} remains the late-time attractor. For $\gamma^2 > 6$, P_{SF} no longer belongs to the physical phase space.

Consequently, no range of γ yields the standard sequence inflation $\to$ graceful exit $\to$ radiation domination within this minimal model. The numerical trajectories discussed below illustrate this analytic fixed-point structure rather than establishing it.



(**a**) $\gamma = 0$ (**b**) $\gamma = 1$ (**c**) $\gamma^2 = 4.2$

(**d**) $\gamma = 0$ (**e**) $\gamma = 1$ (**f**) $\gamma^2 = 4.2$

Figure 1. Phase-space portraits of the autonomous system (66)–(68) for the regular positive branch, $s = +1$. The upper row shows the three-dimensional phase-space trajectories, while the lower row shows their corresponding projections on the x–z plane. Panels (**a**,**d**) correspond to $\gamma = 0$, panels (**b**,**e**) to $\gamma = 1$, and panels (**c**,**f**) to $\gamma^2 = 4.2$. In particular, the plotted region in (**b**) should be understood as a finite visualization window rather than as the full physical phase space. Since the $s = +1$ domain is non-compact in the scalar variables as $x \to 1^-$, some relevant asymptotic boundary configurations can lie outside the displayed box. For example, for $\gamma = 1$, $P_{g\phi}$ has $z \simeq 1.02$, slightly outside the plotted interval. The dynamical trajectories are shown in blue, the critical points are marked by red spheres, and the reddish-orange surface corresponds to $q = 0$, which separates accelerated and decelerated regions of the phase space. This surface is determined by the relation $u^2 - 2z^2 = -1 + \frac{sx}{1-x}$. For the first two cases, with $\gamma^2 \leq 4$, the model exhibits a cascade-like behavior, whereas for $\gamma^2 > 4$, the trajectories approach a decelerated radiation-scalar scaling regime.

In particular, for $\gamma^2 = 0$, the numerical trajectory approaches a de Sitter configuration with $q = -1$. This limit should be understood in terms of the de Sitter critical manifold rather than as an isolated fixed point; in the negative-coupling branch, its geometric endpoint is P_{gdS}. As discussed above, however, this branch is dynamically separated by the degenerate surface $x = 1/4$, where $F'(H) = 0$. For $\gamma^2 = 1$, the trajectory approaches the scalar-field-dominated point P_{SF}, for which $q = \gamma^2/2 - 1 = -1/2$. For $\gamma^2 = 4.2$, the future attractor is instead the scalar–radiation scaling point P_{SS}, with $q = 1$. These numerical trajectories illustrate the analytic fixed-point classification and the absence of a standard graceful exit: the cubic sector may generate an initial accelerated stage, but the asymptotic regime is determined by the scalar slope γ and does not lead, in the minimal model, to a standard post-inflationary radiation era.

We finally stress that the existence of these high-curvature geometric accelerated backgrounds is a statement about the homogeneous and isotropic FLRW background of the cubic truncation. It does not by itself establish their full physical viability. In particular, the anisotropic instability discussed in [29] may affect the robustness of the corresponding high-curvature accelerated backgrounds. Since the scalar field considered here is minimally coupled, its inclusion does not by itself guarantee that an instability intrinsic to the cubic higher-curvature sector is removed. Therefore, if the instability is intrinsic to the cubic geometric sector, it is not automatically cured by the presence of the scalar field. The critical points discussed above should consequently be understood as background solutions of the truncated FLRW system, while their stability under anisotropic perturbations remains a separate requirement.

5.2. Hubble-Flow Diagnostics and Slow-Roll Behavior

In view of the preceding analytic and dynamical results, Figure 2 should be interpreted only as an illustration based on the standard first-order GR-based Hubble-flow mapping. The interval $50 \leq \eta \leq 60$ is not counted backward from a dynamically generated end of inflation, because the minimal model does not provide a standard graceful exit. It is therefore used only as a late-time diagnostic interval along representative background trajectories. At the background level, we evaluate the Hubble-flow parameters defined in Equation (93) along representative trajectories of the autonomous system. In this subsection, we restrict the analysis to the regular positive branch, $s = +1$, since the negative branch is dynamically obstructed by the finite-curvature singular hypersurface at $x = 1/4$. We describe the parameter space in terms of the dimensionless initial geometric strength B and the constant logarithmic slope γ of the exponential scalar potential, with the initial scalar variables held fixed.

Figure 2 summarizes the behavior of the Hubble-flow parameters and of the corresponding GR-based inflationary diagnostics. More specifically, the upper-left panel shows the early-time evolution of ϵ_1 during the geometrically driven stage, while the upper-middle panel shows its behavior during the late-time diagnostic interval. The upper-right panel translates this behavior into the tensor-to-scalar ratio r, showing that smaller values of γ reduce r, although none of the representative trajectories reaches the adopted bound $r_{0.05} < 0.036$. The lower-left panel, however, shows that ϵ_2 remains too small throughout the relevant window, thereby keeping the scalar spectral index too close to exact scale invariance, as illustrated in the lower-middle panel. Finally, the lower-right panel, corresponding to the r–n_s plane, provides the clearest summary of the result: none of the representative trajectories enters the region in which both r and n_s satisfy the adopted bounds. The first relevant feature is the initial accelerated stage generated by the high-curvature cubic contribution. For sufficiently large values of B, the initial conditions place the trajectory in a region where the cubic correction is dynamically important. For the non-phantom trajectories considered here, $Q < 0$, and Equation (66) implies

$$x' = 4x(1-x)Q < 0. \tag{100}$$

Thus, as H decreases, the trajectory evolves from the high-curvature region $x \simeq 1$, where $bH^4 \gg 1$, toward smaller values of x.

In the scalar-free limit, $x = 1/2$, equivalently $bH^4 = 1$, marks the boundary $q = 0$. Therefore, once x decreases below $1/2$, the cubic-radiation sector alone can no longer sustain accelerated expansion. In terms of the instantaneous geometric-strength variable $B = bH^4$, this scalar-free acceleration boundary corresponds to $B = 1$. In the complete system, however, the exact acceleration boundary also depends on u and z. Consequently, the scalar field does not necessarily dominate precisely when $x = 1/2$ is crossed: the trajectory

may first enter an intermediate decelerated regime before the scalar potential becomes sufficiently dominant to generate the subsequent accelerated stage. For smaller values of B, the initial geometric stage is weakened or absent. Once the scalar-field-dominated fixed point controls the evolution, the cubic contribution has vanished ($x = 0$), and the corresponding late-time diagnostics become independent of the initial cubic strength. They are then controlled solely by the exponential-potential slope γ.

During the representative interval $50 \leq \eta \leq 60$, some trajectories reach relatively small values of ϵ_1. However, under the standard diagnostic relation $r = 16\epsilon_1$, the adopted bound $r_{0.05} < 0.036$ at 95% CL [33] requires

$$\epsilon_1 < 2.25 \times 10^{-3}. \tag{101}$$

None of the representative trajectories shown in Figure 2 satisfy this threshold. For sufficiently small values of γ, the scalar field evolves slowly and the background approaches a quasi-de Sitter regime, but ϵ_2 approaches zero during the considered interval. Consequently, the scalar spectral index remains too close to exact scale invariance,

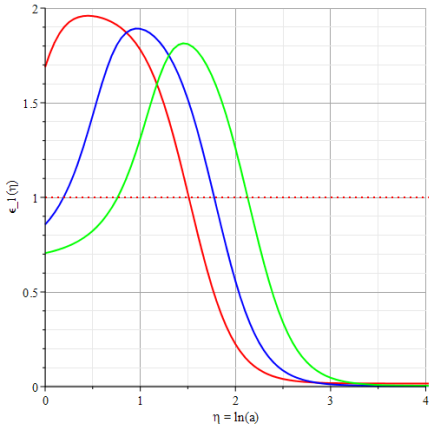
$$n_s \simeq 1 - 2\epsilon_1 - \epsilon_2 \simeq 1. \tag{102}$$

Within the explored regime, decreasing γ further would tend to reduce ϵ_1 and r, but would keep n_s too close to unity, whereas increasing γ modifies the scalar tilt at the cost of increasing ϵ_1 and hence r. Thus, none of the representative trajectories satisfy the adopted bounds on r and n_s simultaneously. Using the former analysis, the scalar-field-dominated fixed point gives $r \simeq 8(1 - n_s)$. This relation is already in strong tension with current constraints on primordial tensor modes. Even if one adopts a higher preferred value of the scalar spectral index, for instance $n_s \simeq 0.974 \pm 0.0034$ at 68%C.L. [34], the power-law relation predicts $r \simeq 8(1 - 0.974) \simeq 0.21$, which remains far above the observational upper bound. Thus, within the adopted first-order GR-based diagnostic, the incompatibility of the minimal exponential scalar-field stage with the tensor bound follows analytically from the power-law relation rather than from the particular representative trajectories.

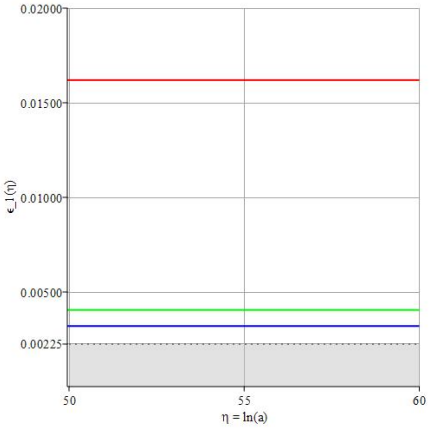
It is important to stress that the $n_s - r$ plane shown in Figure 2 must be interpreted as a GR-based Hubble-flow diagnostic rather than as a full prediction of the modified-gravity model. In higher-curvature gravity, the scalar and tensor spectra may receive corrections from the perturbation sector, and the standard relations used here can be modified by the effective kinetic coefficients, normalization factors, and propagation speeds of the perturbations. Therefore, the present analysis should be understood as a necessary background-level viability test. A definitive comparison with CMB data requires deriving the scalar and tensor perturbation spectra for the cubic geometric sector coupled to radiation and the scalar field.

The absence of trajectories that are simultaneously compatible with ϵ_1, r, and n_s under this diagnostic indicates that the proposed model is dynamically interesting but overly restrictive. Although the positive branch can produce an initially geometrically driven accelerated phase, the fixed H^6 structure of the cubic sector, together with the constant slope of the exponential scalar potential, does not provide sufficient freedom to generate a Hubble-flow hierarchy consistent with the observationally preferred slow-roll pattern.

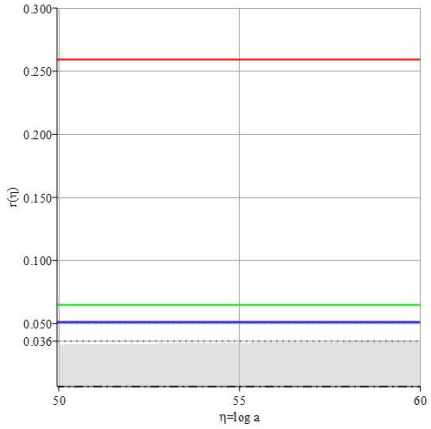
Taken together, the phase-space analysis and the Hubble-flow diagnostics show that the hybrid cubic model generates a nontrivial cascade-like background evolution but fails to reproduce a sufficiently flexible inflationary hierarchy at the diagnostic level considered here. This identifies the minimal cubic realization as a useful benchmark, while also making clear that a more realistic inflationary implementation requires additional freedom in either the scalar or geometric sector.



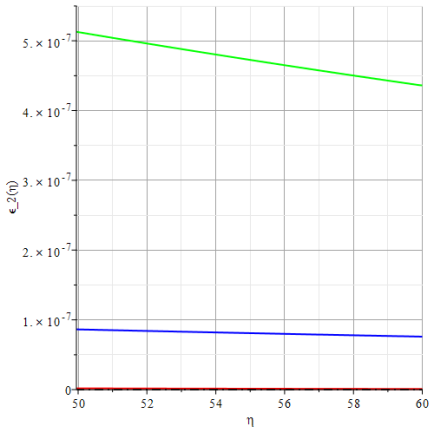
(**a**) Early-time behavior of ϵ_1 during the first 4 e-folds.



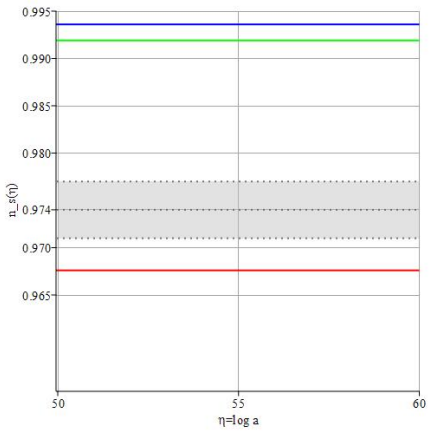
(**b**) Late-time behavior of ϵ_1 during the diagnostic interval $50 \leq \eta \leq 60$.



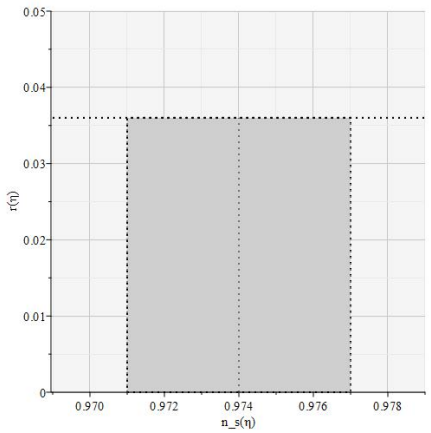
(**c**) Tensor-to-scalar ratio r.



(**d**) Second Hubble-flow parameter ϵ_2.



(**e**) Scalar spectral index n_s.



(**f**) Plane r–n_s.

Figure 2. Hubble-flow parameters and GR-based slow-roll diagnostics for representative trajectories in the (B, γ, u_0, z_0) parameter space. We fix $(u_0, z_0) = (0.002, 0.05)$ and vary (B, γ)The red, blue, and green curves correspond to $(0.1, 0.18)$, $(2, 0.08)$, and $(11, 0.09)$, respectively, for $\beta > 0$. Panel (**a**), display the early-time evolution of ϵ_1, the dashed red line corresponds to $\epsilon_1 = 1$, that is, to the boundary between accelerated and decelerated expansion. The panel (**b**) show the behavior over the late-time diagnostic interval $50 \leq \eta \leq 60$, and the panel (**c**) shows the tensor-to-scalar ratio r. For the lower panel (**d**) show ϵ_2, the panel (**e**) show the scalar spectral index n_s, and the panel (**f**) show the r–(n_s) plane. The shaded regions indicate the adopted observational reference bounds, $r_{0.05} < 0.036$, $\epsilon_1 < 0.00225$, and $n_s = 0.9743 \pm 0.0034$ 68% C.L.), based on BICEP/Keck and ACT DR6 + Planck + DESI DR1. We use these bounds for diagnostic comparisons rather than as a joint confidence region. The trajectories illustrate the analytical constraint associated with the scalar-field-dominated fixed point $P_{\rm SF}$, where $\epsilon_1 = \gamma^2/2$ and $\epsilon_2 = 0$, yielding $r \simeq 8(1 - n_s)$. Consequently, none of the representative trajectories simultaneously satisfies the adopted r and n_s constraints, highlighting the observational limitations of the minimal exponential scalar sector.

6. Conclusions

In this work, we have investigated the background cosmological dynamics of a hybrid model composed of the cubic sector of Geometric Inflation, radiation, and a minimally coupled canonical scalar field with an exponential potential. By introducing a compactified Hubble variable and suitable dimensionless variables for the matter sector, we formulated the cosmological equations as an autonomous dynamical system, classified the finite critical points and their stability, examined the relevant asymptotic behavior of the non-compact

positive-coupling branch, and evaluated the Hubble-flow diagnostics along representative trajectories.

The analysis shows that the cubic correction can generate a geometrically driven accelerated stage at high curvature. In the regular positive-coupling branch, this acceleration occurs when the cubic term dominates sufficiently over the Einstein–Hilbert contribution, namely for $bH^4 > 1$. However, the duration of this geometrically accelerated phase grows only logarithmically with the initial high-curvature hierarchy. In the high-curvature cubic-radiation regime, the leading behavior is

$$N_{\rm geo} \simeq \frac{3}{8} \ln B, \qquad B \equiv bH_0^4,$$

up to a subleading constant correction. Thus, obtaining a sufficiently long geometric stage requires an exponentially large initial hierarchy. Consequently, although the cubic truncation can trigger accelerated expansion, it does not by itself provide enough geometric e-folds to solve the horizon problem for moderate initial values of the high-curvature hierarchy.

The sign of the cubic coupling remains dynamically important. For $\beta < 0$, the system contains a finite-curvature degeneracy at $bH^4 = 1/3$, equivalently $x = 1/4$, where the modified Friedmann map loses local invertibility and the Raychaudhuri equation ceases to determine a regular evolution uniquely. This branch can formally avoid the arbitrarily large radiation densities associated with the positive branch, but only at the price of a branch-separating dynamical obstruction. By contrast, the regular positive-coupling branch avoids this finite-curvature degeneracy but retains the trans-Planckian radiation-density problem in the asymptotic past. In particular, the asymptotic high-curvature configurations P_{gw} and $P_{g\phi}$ satisfy $\Omega_r \to \infty$. Hence, the inclusion of radiation and a minimally coupled scalar field does not cure the radiation-density obstruction of the regular cubic branch.

The scalar-field sector controls the late-time fate of the regular trajectories. At the scalar-field-dominated point P_{SF}, $\epsilon_1 = \gamma^2/2$ is constant, so this regime corresponds to a power-law solution. Within the first-order GR-based Hubble-flow diagnostic used in this work, $\epsilon_2 = 0$ at the fixed point and therefore

$$n_s \simeq 1 - \gamma^2, \qquad r \simeq 8\gamma^2,$$

which implies

$$r \simeq 8(1 - n_s).$$

For the observationally preferred range of the scalar spectral index, this relation predicts a tensor-to-scalar ratio well above the adopted upper bound. Thus, within this GR-based diagnostic, the tension is an analytic consequence of the constant logarithmic slope of the exponential potential rather than a numerical artifact of the representative trajectories.

A further limitation is the absence of a standard graceful exit. For $\gamma = 0$, the constant potential generates de Sitter critical manifolds and there is no dynamical exit from the accelerated state. For $0 < \gamma^2 < 2$, P_{SF} is an accelerated future attractor and the scalar-driven accelerated phase persists asymptotically. At $\gamma^2 = 2$, the solution lies on the acceleration–deceleration boundary, but remains scalar-field-dominated with $\Omega_r = 0$, so this does not represent a transition to a radiation era. For $2 < \gamma^2 < 4$, P_{SF} is a decelerated future attractor, again with $\Omega_r = 0$. At $\gamma^2 = 4$, the scalar-field-dominated and scalar–radiation scaling branches meet. For $\gamma^2 > 4$, the late-time attractor is the scaling point P_{SS}, in which the scalar field tracks radiation and retains a nonzero fractional density for every finite γ. Therefore, no value of γ in the minimal model produces the standard sequence

$$\text{inflation} \longrightarrow \text{graceful exit} \longrightarrow \text{radiation domination}.$$

Accordingly, a nominal interval such as $50 \leq \eta \leq 60$ cannot be interpreted as the last e-folds counted backwards from a dynamically generated end of inflation; it is used here only as a diagnostic interval along representative background trajectories.

These results clarify the division of roles within the hybrid construction. The cubic geometric sector can trigger an initial accelerated epoch, whereas the scalar slope γ determines the asymptotic scalar-field regime. The minimal combination of a cubic curvature correction, radiation, and a canonical scalar field with an exponential potential is nevertheless too restrictive to produce a viable inflationary background. The main obstructions are analytic: the geometrically accelerated stage is too short, the subsequent scalar-field-dominated phase satisfies the power-law relation $r \simeq 8(1 - n_s)$ within the adopted GR-based diagnostic, and no value of γ yields a standard graceful exit into a radiation-dominated post-inflationary epoch.

The non-compact structure of the positive branch does not alter these conclusions. Our asymptotic analysis shows that, for $\gamma \neq 0$, the candidate stationary directions at $u^2 + z^2 \to \infty$ are kinetic-dominated and do not generate an additional quasi-de Sitter future attractor. For $\gamma = 0$, the non-compact boundary instead contains the asymptotic continuation of the de Sitter critical manifold. Thus, although the analysis does not constitute a complete Poincaré compactification of the three-dimensional system, the relevant non-compact asymptotic behavior does not provide an additional mechanism capable of overcoming the inflationary obstructions identified above.

Finally, the interpretation of the model remains limited by issues that go beyond homogeneous FLRW dynamics. The geometrically accelerated high-curvature stage occurs precisely where the cubic term becomes important relative to the Einstein–Hilbert contribution, so the domain of validity of the cubic truncation must ultimately be assessed within a controlled higher-curvature completion. Moreover, the existence and stability of the homogeneous critical points do not establish perturbative or anisotropic stability. In particular, the anisotropic instability previously reported for the cubic geometric sector must be revisited in the full scalar–radiation–geometry system. Since the scalar field considered here is minimally coupled, its inclusion does not by itself guarantee that an instability intrinsic to the cubic higher-curvature sector is removed.

Accordingly, the present work should be interpreted as a background-level analysis of the possibilities and limitations of the minimal hybrid cubic scenario. Its main result is negative but informative: the cubic truncation admits geometric-to-scalar cascade-like trajectories at the level of homogeneous dynamics, but this minimal realization does not satisfy the background requirements of a viable inflationary cosmology. A successful extension would require additional structure, such as a controlled higher-curvature tower, a scalar potential with a field-dependent logarithmic slope or a genuine exit mechanism, a consistent reheating channel into radiation, and a perturbatively stable scalar–tensor sector.

Author Contributions: Conceptualization, R.G.-S. and L.N.-C.; methodology, L.N.-C. and R.G.-S.; software, L.N.-C.; validation, I.Q., J.A.V. and R.G.-S.; formal analysis, L.N.-C., R.G.-S. and J.A.V.; investigation, L.N.-C. and R.G.-S.; data curation, L.N.-C.; writing—original draft preparation, L.N.-C. and R.G.-S.; writing—review and editing, L.N.-C., J.A.V., I.Q. and R.G.-S.; visualization, L.N.-C.; supervision, R.G.-S. and I.Q.; project administration, R.G.-S.; funding acquisition, J.A.V., I.Q. and R.G.-S. All authors have read and agreed to the published version of the manuscript.

Funding: This research was funded by: FORDECYT-PRONACES-CONACYT project CF-MG-2558591 grant, Secretaría de Investigación y Posgrado, Instituto Politécnico Nacional, grant numbers SIP20250043 and MULTI-2026-0004-M3. J.A.V. acknowledges support from FOSEC SEP-CONACYT Ciencia Básica A1-S-21925, UNAM-DGAPA-PAPIIT IN117723, IN110325, and Cátedra de Investigación Marcos Moshinsky.

Data Availability Statement: The numerical data generated in this study, together with the scripts used to integrate the autonomous dynamical system and to produce the phase-space and Hubble-flow figures, are available from the corresponding author upon reasonable request. No external datasets were used in this study.

Acknowledgments: During the preparation of this manuscript, the authors used Gemini 3.5 Flash for English translation and proofreading. The authors have reviewed and edited the output and take full responsibility for the content of this publication.

Conflicts of Interest: The authors declare no conflicts of interest.

Abbreviations

The following abbreviations are used in this manuscript:

NEC	Null energy condition
WEC	Weak energy condition
SEC	Strong energy condition
DEC	Dominant energy condition
GQTG	Generalized Quasi-Topological Gravities
GC	Geometric Cosmology
FLRW	Friedmann-Lemaître-Robertson-Walker
CECG	Cosmological Einsteinian Cubic Gravity
GI	Geometric Inflation
GR	General Relativity
CMB	Cosmic Microwave Background

References

1. Uzan, J.P. Inflation in the standard cosmological model. *Comptes Rendus. Phys.* **2015**, *16*, 875–890. [CrossRef]
2. Guth, A.H. Inflationary universe: A possible solution to the horizon and flatness problems. *Phys. Rev. D* **1981**, *23*, 347–356. [CrossRef]
3. Linde, A.D. A New Inflationary Universe Scenario: A Possible Solution of the Horizon, Flatness, Homogeneity, Isotropy and Primordial Monopole Problems. *Phys. Lett. B* **1982**, *108*, 389–393. [CrossRef]
4. Akrami, Y.; Arroja, F.; Ashdown, M.; Aumont, J.; Baccigalupi, C.; Ballardini, M.; Banday, A.J.; Barreiro, R.; Bartolo, N.; Basak, S.; et al. Planck 2018 results-X. Constraints on inflation. *Astron. Astrophys.* **2020**, *641*, A10.
5. Peebles, P.J.E.; Yu, J.T. Primeval Adiabatic Perturbation in an Expanding Universe. *Astrophys. J.* **1970**, *162*, 815–836. [CrossRef]
6. Sunyaev, R.A.; Zel'dovich, Y.B. Small-Scale Fluctuations of Relic Radiation. *Astrophys. Space Sci.* **1970**, *7*, 3–19. [CrossRef]
7. Battefeld, D.; Peter, P. A Critical Review of Classical Bouncing Cosmologies. *Phys. Rep.* **2015**, *571*, 1–66. [CrossRef]
8. Brandenberger, R.; Peter, P. Bouncing Cosmologies: Progress and Problems. *Found. Phys.* **2017**, *47*, 797–850. [CrossRef]
9. Martin, J.; Brandenberger, R.H. The Trans-Planckian Problem of Inflationary Cosmology. *Phys. Rev. D* **2001**, *63*, 123501. [CrossRef]
10. Amin, M.A.; Hertzberg, M.P.; Kaiser, D.I.; Karouby, J. Nonperturbative Dynamics Of Reheating After Inflation: A Review. *Int. J. Mod. Phys. D* **2015**, *24*, 1530003. [CrossRef]
11. Martin, J. Inflation after Planck: And the winners are. *arXiv* **2013**, arXiv:1312.3720.
12. Ijjas, A.; Steinhardt, P.J.; Loeb, A. Inflationary paradigm in trouble after Planck2013. *Phys. Lett. B* **2013**, *723*, 261–266. [CrossRef]
13. Starobinsky, A.A. A New Type of Isotropic Cosmological Models Without Singularity. *Phys. Lett. B* **1980**, *91*, 99–102. [CrossRef]
14. Stelle, K.S. Renormalization of Higher-Derivative Quantum Gravity. *Phys. Rev. D* **1977**, *16*, 953–969. [CrossRef]
15. Zwiebach, B. Curvature Squared Terms and String Theories. *Phys. Lett. B* **1985**, *156*, 315–317. [CrossRef]
16. Bueno, P.; Cano, P.A.; Hennigar, R.A. (Generalized) quasi-topological gravities at all orders. *Class. Quantum Gravity* **2020**, *37*, 015002. [CrossRef]
17. Bueno, P.; Cano, P.A.; Hennigar, R.A.; Lu, M.; Moreno, J. Generalized quasi-topological gravities: The whole shebang. *Class. Quantum Gravity* **2023**, *40*, 015004. [CrossRef]
18. Moreno, J.; Murcia, A.J. Cosmological higher-curvature gravities. *Class. Quantum Gravity* **2024**, *41*, 135017. [CrossRef]
19. Arciniega, G.; Bueno, P.; Cano, P.A.; Edelstein, J.D.; Hennigar, R.A.; Jaime, L.G. Cosmic inflation without inflaton. *Int. J. Mod. Phys. D* **2019**, *28*, 1944008. [CrossRef]
20. Arciniega, G.; Bueno, P.; Cano, P.A.; Edelstein, J.D.; Hennigar, R.A.; Jaime, L.G. Geometric inflation. *Phys. Lett. B* **2020**, *802*, 135242. [CrossRef]

21. Jaime, L.G.; Arciniega, G. A unified geometric description of the Universe: From inflation to late-time acceleration without an inflaton nor a cosmological constant. *Phys. Lett. B* **2022**, *827*, 136939. [CrossRef]
22. Arciniega, G.; Jaime, L.G.; Landau, S.J.; Leizerovich, M. On Geometric Cosmology. *arXiv* **2025**, arXiv:2504.00124.
23. Arciniega, G.; Edelstein, J.D.; Jaime, L.G. Towards geometric inflation: The cubic case. *Phys. Lett. B* **2020**, *802*, 135272. [CrossRef]
24. Quiros, I.; García-Salcedo, R.; Gonzalez, T.; Martínez, J.L.M.; Nucamendi, U. Global asymptotic dynamics of cosmological Einsteinian cubic gravity. *Phys. Rev. D* **2020**, *102*, 044018. [CrossRef]
25. Quiros, I.; De Arcia, R.; García-Salcedo, R.; Gonzalez, T.; Cedeno, F.X.L.; Nucamendi, U. Quantum origin of inflation in the geometric inflation model. *Phys. Rev. D* **2021**, *103*, 064043. [CrossRef]
26. Arciniega, G.; Jaime, L.G.; Piccinelli, G. Inflationary predictions of geometric inflation. *Phys. Lett. B* **2020**, *809*, 135731. [CrossRef]
27. Leizerovich, M.; Jaime, L.G.; Landau, S.J.; Arciniega, G. Geometric Cosmology models: Statistical analysis with observational data. *Universe* **2026**, *12*, 129. [CrossRef]
28. Edelstein, J.D.; Rodriguez, D.V.; López, A.V. Aspects of geometric inflation. *J. Cosmol. Astropart. Phys.* **2020**, *2020*, 040. [CrossRef]
29. Pookkillath, M.C.; De Felice, A.; Starobinsky, A.A. Anisotropic instability in a higher order gravity theory. *J. Cosmol. Astropart. Phys.* **2020**, *2020*, 041. [CrossRef]
30. Bueno, P.; Cano, P.A. Einsteinian cubic gravity. *Phys. Rev. D* **2016**, *94*, 104005. [CrossRef]
31. Schwarz, D.J.; Terrero-Escalante, C.A.; García, A.A. Higher order corrections to primordial spectra from cosmological inflation. *Phys. Lett. B* **2001**, *517*, 243–249. [CrossRef]
32. Leach, S.M.; Liddle, A.R.; Martin, J.; Schwarz, D.J. Cosmological parameter estimation and the inflationary cosmology. *Phys. Rev. D* **2002**, *66*, 023515. [CrossRef]
33. Ade, P.A.R.; Ahmed, Z.; Amiri, M.; Barkats, D.; Thakur, R.B.; Bischoff, C.A.; Beck, D.; Bock, J.J.; Boenish, H.; Bullock, E.; et al. [BICEP/Keck Collaboration] Improved Constraints on Primordial Gravitational Waves using Planck, WMAP, and BICEP/Keck Observations through the 2018 Observing Season. *Phys. Rev. Lett.* **2021**, *127*, 151301. [CrossRef]
34. Louis, T.; La Posta, A.; Atkins, Z.; Jense, H.T.; Abril-Cabezas, I.; Addison, G.E.; Ade, P.A.R.; Aiola, S.; Alford, T.; Alonso, D.; et al. The Atacama Cosmology Telescope: DR6 power spectra, likelihoods and ΛCDM parameters. *J. Cosmol. Astropart. Phys.* **2025**, *11*, 62. [CrossRef]

Disclaimer/Publisher's Note: The statements, opinions and data contained in all publications are solely those of the individual author(s) and contributor(s) and not of MDPI and/or the editor(s). MDPI and/or the editor(s) disclaim responsibility for any injury to people or property resulting from any ideas, methods, instructions or products referred to in the content.